March 1987
LU TP 87-5

A Multiple Interaction Model for the Event Structure in Hadron Collisions

Torbjörn Sjöstrand, Maria van Zijl
Department of Theoretical Physics,
University of Lund, Sölvegatan 14A,
S-223 62 Lund, Sweden

Abstract:

A detailed model for hadronic events is presented, with particular emphasis put on the event structure at low transverse momenta, i.e. "beam jets" and "minijets". Specifically, we argue that hadronic events contain a varying number of semihard parton-parton interactions, with average interaction rate given by perturbative QCD, and the variation between different events by Poissonian statistics for each impact parameter separately. Comparisons with data are presented for a number of properties, such as multiplicity distributions, forward-backward correlations, minijet phenomenology and the "pedestal effect". Also predictions for the behaviour at higher energies are included.

1. Introduction

In current hadron colliders, the interaction between two incoming hadrons typically results in the production of ten to a hundred outgoing particles. We have every reason to believe that this process is described by the standard model for strong and electroweak phenomena. Unfortunately, a correct quantum mechanical treatment does not seem to be within reach, both because of the sheer number of particles involved and because of the limited understanding of nonperturbative QCD. We are therefore in an upside-down situation where the rare processes, like W/Z or high-p_T jet production, are the easiest to understand: since they involve large momentum transfers, they are also amenable to perturbative analysis. Typical minimum bias events, which appear with large cross-sections, offer no such handle.

The best that can be done at present is to try to develop simplified models. In order to account for the phenomenology already known, these models still have to be of a considerable complexity, as we shall see. In general terms, the components needed include the generation of a hard interaction by a convolution of (i) hard scattering matrix elements and (ii) structure functions; the addition of (iii) initial state and (iv) final state radiation; the inclusion of (v) beam jets; and, finally, (vi) the fragmentation of partons into hadrons and the subsequent decay of unstable hadrons. Among these subjects, the structure of beam jets is certainly the least well understood.

The objective of the present paper is to develop one particular scenario for strong interaction physics at hadron colliders (elastic and diffractive events excepted). Our basic philosophy will be as follows [1,2]. The total rate of parton-parton interactions, as a function of the transverse momentum scale p_T, is assumed to be given by perturbative QCD. This is certainly true for reasonably large p_T values, but in this paper we shall also extend the perturbative parton-parton scattering framework into the low-p_T region. A regularization of the divergence in the cross-section for $p_T \to 0$ has to be introduced, however, which will provide us with one of the main free parameters of the model. Since each incoming hadron is a composite object, consisting of many partons, the possibility of several parton pairs interacting when two hadrons collide should exist. It is not unreasonable to assume that the different pairwise interactions take place essentially

independently of each other, and that therefore the number of interactions in a collision is given by a Poissonian distribution. Furthermore, hadrons are not only composite but also extended objects, meaning that collisions range from very central to rather peripheral ones. Reasonably, the average number of interactions should be larger in the former than in the latter case. Whereas the assumption of a Poissonian distribution should hold for each impact parameter separately, the distribution in number of interactions should be widened by the spread of impact parameters. The amount of widening will depend on the assumed matter distribution inside the colliding hadrons. Different possibilities will be compared.

The proposed route is not an easy one. It leads to a fairly complex scenario, which may make the resulting model look unattractive. However, the world of hadron physics *is* complicated, and if we err, it is most likely in being too unsophisticated. The experience gained with the model, in failures as well as successes, could be used as a guideline in the evolution of yet more detailed models.

The complexity of the model excludes the possibility of obtaining significant information by analytical techniques. Rather, the model has been implemented within the framework of the Lund Monte Carlo programs, using PYTHIA version 4.8 [3] for points (i), (ii), (iii) and (v) above, and JETSET version 6.3 [4] for (iv) and (vi). These programs are publicly available and can be used e.g. to study implications for a given detector setup.

To the best of our knowledge, a scenario like the one outlined above has not been studied before. Yet, none of the individual ideas is new. A number of authors have studied the probability of having two hard interactions in an event [5-7], in particular for the production of (three or) four high-p_T jets. Within the framework of Dual Topological Unitarization (DTU) [8-11], the variation in the number of cut Pomerons corresponds to our variation in the number of semihard interactions. The difference is that DTU is a nonperturbative approach, which describes the longitudinal structure of particle production. Transverse degrees of freedom can be added [10], but this is not an integral part of the framework. Put drastically, our approach is an attempt to extend a perturbative, high-p_T picture down into the low-p_T region, whereas the DTU approach provides a low-p_T model that could be extended to higher p_T values. Also the effects of varying impact parameters have been studied with respect to multiplicity distributions and forward-backward correlations [12], and with respect to the increase in total cross-section and

the "blackening" of the proton with increasing energy [13]. No detailed studies have been done within the framework of multiple parton interactions, however.

The idea of multiple interactions has gained experimental support by the recent AFS study of four-jet events [14]. The kinematics of these events indicates that, while some of them can be attributed to a single hard scattering with associated bremsstrahlung, a fair fraction contains two hard interactions. While no direct comparisons are made with the AFS signal, a few general comments are given in section 6.2.

The outline of the paper is as follows. In section 2 the general formalism of multiple interactions is outlined, without the complication of variable impact parameters. The resulting model, as well as models without any multiple interactions at all, are compared with data in section 3, and some areas of discrepancy are noted. Part of the material in these two sections is taken from [1]. A variable impact parameter picture of hadronic interactions is introduced in section 4, together with necessary modifications of the multiple interaction formalism. The phenomenology of the resulting model is covered in sections 5 and 6, in the former for multiplicity distributions and in the latter for jet properties. A summary and outlook is given in section 7.

2. The Impact Parameter Independent Model

2.1. The QCD Jet Cross-Section

The natural starting point for our deliberations is provided by the perturbative QCD cross-section for parton-parton interactions

$$\sigma = \sum_{i,j,k} \iiint dx_1\, dx_2\, d\hat{t}\; \hat{\sigma}^k_{ij}(\hat{s},\hat{t},\hat{u})\; f^1_i(x_1,Q^2)\; f^2_j(x_2,Q^2). \tag{1}$$

Here $\hat{\sigma}^k_{ij}$ is the hard scattering cross-section for the k:th subprocess possible between incoming partons i and j. The structure functions $f^a_i(x,Q^2)$ give the probability for finding a parton i carrying a fraction x of the energy (and longitudinal momentum) of the incoming hadron a, if the hadron is probed at a scale Q^2. For massless partons, the three Mandelstam variables are related by $\hat{s} + \hat{t} + \hat{u} = 0$, and $\hat{s} = x_1 x_2 s$. While the $\hat{\sigma}$ are calculable in perturbative QCD (see e.g. [15]), the structure functions are not. In the following we have chosen to use EHLQ set 1 [15], with $\Lambda = 0.2$ GeV. The Q^2 scale, which is also ambiguous, has been set to

$$Q^2 = p_T^2 = \frac{\hat{t}\hat{u}}{\hat{s}}. \tag{2}$$

In the study of absolute jet cross-sections, it will become necessary to introduce a K-factor, to account for higher order corrections to the lowest order $\hat{\sigma}^k_{ij}$ results. This can be done in several different ways. In [16] it has been shown that a reasonable approximation to first order corrections is to replace the $\alpha_s(p_T^2)$ in the $\hat{\sigma}^k_{ij}$:s by $\alpha_s(0.075 \cdot p_T^2)$; this is the recipe that will be adopted when needed.

A reasonable measure for the "hardness" of a parton-parton interaction is provided by the p_T^2 scale. The differential cross-section as a function of p_T^2 is given by

$$\frac{d\sigma}{dp_T^2} = \sum_{i,j,k} \iiint dx_1\, dx_2\, d\hat{t}\; \hat{\sigma}^k_{ij}(\hat{s},\hat{t},\hat{u})\; f^1_i(x_1,Q^2)\; f^2_j(x_2,Q^2)\; \delta(p_T^2 - \frac{\hat{t}\hat{u}}{\hat{s}}) \tag{3}$$

and the hard scattering cross-section above some p_{Tmin} by

$$\sigma_{hard}(p_{Tmin}) = \int_{p_{Tmin}^2}^{s/4} \frac{d\sigma}{dp_T^2}\, dp_T^2. \tag{4}$$

Since the differential cross-section diverges roughly like dp_T^2/p_T^4, σ_{hard} is also divergent for $p_{Tmin} \to 0$. This is illustrated in Fig. 1 for a few different CM energies.

There are two potential major sources of error to the results in Fig. 1. Firstly, the "dense packing" problem [17]: at small x values the effective number of partons in a hadron can grow so fast that not all fit inside the hadron. Then parton recombination effects become important, and the standard Altarelli-Parisi evolution of structure functions is no longer valid. Fortunately, it has been shown [18] that p_{Tmin} values around or above 2 GeV are safe all the way up to SSC energies. Secondly, the shape of the structure functions at small x and small Q^2 values is given neither by experiment nor by theory. Different reasonable ansätze could well give an order of magnitude difference for the $\sigma_{hard}(p_{Tmin} = 2\text{ GeV})$ at 40 TeV [19]. In our calculations, the effective shape at small x is roughly x^{-1}, but arguments have been raised for a behaviour more like $x^{-1.3}$ [20].

At present collider energies, $\sigma_{hard}(p_{Tmin})$ becomes comparable with the total cross-section for $p_{Tmin} \approx 1.5 - 2$ GeV. This need not lead to contradictions: σ_{hard} does not give the hadron-hadron cross-section but the parton-parton one. Each of the incoming hadrons may be viewed as a beam of partons, with the possibility of having several parton-parton interactions when the hadrons pass through each other. In this language, $\sigma_{hard}(p_{Tmin})/\sigma_{tot}$ is simply the average number per event of parton-parton scatterings above p_{Tmin}, and this number may well be larger than unity.

While the introduction of several interactions per event is the natural consequence of allowing small p_{Tmin} values and hence large σ_{hard} ones, it is not the solution of $\sigma_{hard}(p_{Tmin})$ being divergent for $p_{Tmin} \to 0$: the average $\hat{s}$ of a scattering decreases slower with p_{Tmin} than the number of interactions increases, so naively the total amount of scattered partonic energy becomes infinite. One cutoff is therefore obtained via the need to introduce proper multi-parton correlated structure functions inside a hadron. This is not a part of the standard perturbative QCD formalism and is therefore not built into eq. (4). In practice, it seems to be too weak a cut, i.e. it leads to a picture with too little of the incoming energy remaining in the small-angle beam jet region.

A more credible reason for an effective cutoff is that the incoming hadrons are colour neutral objects. Therefore, when the p_T of an exchanged gluon is made small and the transverse wavelength correspondingly large, the gluon can no longer resolve the individual colour charges, and the effective coupling is decreased. This mechanism is not in contradiction to perturbative QCD calculations, which are always performed assuming scattering of free partons (rather than partons inside hadrons), but neither does present knowledge of QCD provide an understanding of how such a decoupling mechanism would work in detail. For the purpose of this section, a sharp cutoff at some energy-independent p_{Tmin} scale will be used, i.e. it will be assumed that $d\sigma/dp_T^2 = 0$ for $p_T < p_{Tmin}$. The issue will be further discussed in section 4.

Finally, a word about total cross-sections. The σ_{tot} of hadron-hadron interactions is conveniently subdivided into a number of terms

$$\sigma_{tot}(s) = \sigma_{el}(s) + \sigma_{sd}(s) + \sigma_{dd}(s) + \sigma_{nd}(s) \tag{5}$$

where σ_{el} is the elastic cross-section, σ_{sd} the single diffractive one, σ_{dd} the double diffractive one and σ_{nd} the nondiffractive, inelastic one. It is the latter class of "ordinary multihadronic events" that this paper sets out

to study, and a knowledge of $\sigma_{nd}(s)$ is therefore required. In this paper we have used the Block-Cahn set 1 parametrization for $\sigma_{tot}(s)$ and $\sigma_{el}(s)$ [21], and diffractive cross-sections are given by the ansatz of Goulianos [22]. This leaves a σ_{nd} of roughly 40 mb at 600 GeV and 100 mb at 40 TeV.

2.2. The Multiple Interaction Formalism

In an event with several interactions, it is convenient to impose an ordering. The logical choice is to arrange the scatterings in falling sequence of $x_T = 2p_T/s^{1/2}$. The "first" scattering is thus the hardest one, with the "subsequent" ("second", "third", etc.) successively softer. It is important to remember that this terminology is in no way related to any picture in physical time; we do not know anything about the latter. In principle, all the scatterings that occur in an event must be correlated somehow, naively by momentum and flavour conservation for the partons from each incoming hadron, less naively by various quantum mechanical effects. When averaging over all configurations of soft partons, however, one should effectively obtain the standard QCD phenomenology for a hard scattering, e.g. in terms of tructure functions. Correlation effects, known or estimated, can be introduced in the choice of subsequent scatterings, given that the "preceding" (harder) ones are already known.

With a total cross-section of hard interactions $\sigma_{hard}(p_{Tmin})$ to be distributed among $\sigma_{nd}(s)$ (nondiffractive, inelastic) events, the average number of interactions per event is just the ratio $\sigma_{hard}(p_{Tmin})/\sigma_{nd}(s)$. As a starting point we will assume that all hadron collisions are equivalent (no impact parameter dependence), and that the different parton-parton interactions take place completely independently of each other. The number of scatterings per event is then distributed according to a Poissonian with mean $\sigma_{hard}(p_{Tmin})/\sigma_{nd}(s)$. For Monte Carlo generation of these interactions it is useful to define

$$p(x_T) = \frac{1}{\sigma_{nd}(s)} \frac{d\sigma}{dx_T}, \tag{6}$$

with $d\sigma/dx_T$ obtained by analogy with eq. (3). Then $p(x_T)$ is simply the probability to have a parton-parton interaction at x_T, given that the two hadrons undergo a nondiffractive, inelastic collision.

The probability that the hardest interaction, i.e. the one with highest x_T, is at x_{T1}, is now given by

$$p(x_{T1}) \exp\{-\int_{x_{T1}}^{1} p(x_T')\, dx_T'\}, \tag{7}$$

i.e. the naive probability to have a scattering at x_{T1} multiplied by the probability that there was no scattering with x_T larger than x_{T1}. Correspondingly, the probability to have the second hardest scattering at x_{T2} is given by

$$\begin{aligned} &\int_{x_{T2}}^{1} dx_{T1} \exp\{-\int_{x_{T1}}^{1} p(x_T')\, dx_T'\}\, p(x_{T1}) \exp\{-\int_{x_{T2}}^{x_{T1}} p(x_T')\, dx_T'\}\, p(x_{T2}) = \\ &= p(x_{T2}) \{\int_{x_{T2}}^{1} p(x_T')\, dx_T'\} \exp\{-\int_{x_{T2}}^{1} p(x_T')\, dx_T'\}, \end{aligned} \tag{8}$$

i.e. the product of the probabilities to have no scattering between 1 and x_{T1}, to have one at x_{T1}, to have none between x_{T1} and x_{T2} and to have one at x_{T2}, integrated over all possible x_{T1}. In general, for the n:th scattering, the exponentials always sum up to give the integral between x_{Tn} and 1. The nested integral over scatterings $x_{T1} > x_{T2} > \ldots\ldots > x_{T(n-1)} > x_{Tn}$ is given by

$$\begin{aligned} &\int_{x_{Tn}}^{1} dx_{T1}\, p(x_{T1}) \int_{x_{Tn}}^{x_{T1}} dx_{T2}\, p(x_{T2}) \ldots\ldots \int_{x_{Tn}}^{x_{T(n-2)}} dx_{T(n-1)}\, p(x_{T(n-1)}) = \\ &= \frac{1}{(n-1)!} \{\int_{x_{Tn}}^{1} p(x_T')\, dx_T'\}^{n-1}, \end{aligned} \tag{9}$$

so that the probability for a n:th scattering at x_{Tn} becomes

$$p(x_{Tn}) \frac{1}{(n-1)!} \{\int_{x_{Tn}}^{1} p(x_T')\, dx_T'\}^{n-1} \exp\{-\int_{x_{Tn}}^{1} p(x_T')\, dx_T'\}. \tag{10}$$

The total probability to have a scattering at x_T, irrespectively of it being the first, second or whatever, obviously is

$$\sum_{n=1}^{\infty} p(x_T) \frac{1}{(n-1)!} \{\int_{x_T}^{1} dx_T'\, p(x_T')\}^{n-1} \exp\{-\int_{x_T}^{1} dx_T'\, p(x_T')\} = p(x_T). \tag{11}$$

The multiple interaction formalism thus retains the correct perturbative QCD expression for the scattering probability at any given x_T.

With the help of the integral

$$P(x_T) = \int_{x_T}^{1} p(x_T')\, dx_T' = \frac{1}{\sigma_{nd}} \int_{sx_T^2/4}^{s/4} \frac{d\sigma}{dp_T^2}\, dp_T^2 \tag{12}$$

(where we assume $P(x_T) \to \infty$ for $x_T \to 0$) and its inverse P^{-1}, the iterative procedure to generate a chain of scatterings $x_{T1} > x_{T2} > \ldots\ldots$ is described by

$$x_{Ti} = P^{-1}\{P(x_{T(i-1)}) - \ln R_i\}. \tag{13}$$

Here the R_i are random numbers evenly distributed between 0 and 1. The iterative chain is started with a fictitious $x_{T0} = 1$ and is terminated when x_{Ti} is smaller than $x_{Tmin} = 2p_{Tmin}/s^{1/2}$. Since P and P^{-1} are not known analytically, the standard Monte Carlo procedure is to find a $\tilde{p}(x_T) \geq p(x_T)$ for all $x_T > x_{Tmin}$, with $\tilde{p}$ a particularly simple function, like constant/x_T^3 (i.e. using the approximate dp_T^2/p_T^4 behaviour noted earlier), which can be analytically integrated and inverted. From the chain generated with the use of $\tilde{p}(x_T)$, a given x_{Ti} is to be retained with probability $p(x_{Ti})/\tilde{p}(x_{Ti})$.

In addition, for each x_T value chosen, further variables have to be found according to the matrix element. This involves selecting $\tau = x_1 x_2$ and $x_F = x_1 - x_2$ for each incoming parton pair, resolving the twofold ambiguity between $\hat{t}$ and x_T

$$\hat{t} = -\frac{1}{2}\hat{s}\, \{1 \pm (1 - \frac{x_T^2}{\tau})^{1/2}\}, \tag{14}$$

choosing flavours for the incoming partons and, where necessary, for the outgoing ones. All this can be handled using standard Monte Carlo techniques, in particular by generalizing $p(x_T)$ and $\tilde{p}(x_T)$ above to be functions also of τ, x_F etc.

Whereas the ordinary structure functions should be used for the hardest scattering in order to reproduce standard QCD phenomenology, the structure functions to be used for subsequent scatterings must depend on all preceding x values and flavours chosen. We do not know enough about the hadron wave function to write down such joint probability distributions (some suggestions are found in [23, 24, 6, 7]). To take into account the energy "already" used in harder scatterings, a conservative approach is to evaluate the structure functions, not at x_n^a for the n:th scattered parton from hadron a but at

$$x_n'^a = \frac{x_n^a}{1 - \sum_{i=1}^{n-1} x_i^a}. \tag{15}$$

This will be our standard procedure in the following; we have tried a few alternatives without finding any significantly different behaviour in the final physics.

2.3. Further Model Details

In a fraction $\exp(-P(x_{Tmin}))$ of the events studied, there will be no hard scattering above x_{Tmin} when the iterative procedure in eq. (13) is applied. It is therefore also necessary to have a model for what happens in events with no (semi)hard interactions. The simplest possible way to produce an event is to have an exchange of a very soft gluon between the two colliding hadrons. Without (initially) affecting the momentum distribution of partons, the "hadrons" become colour octet objects rather than colour singlet ones. If only valence quarks are considered, the colour octet state of a baryon can be decomposed into a colour triplet quark and an antitriplet diquark. In a baryon-baryon collision, one would then obtain a two-string picture [25], with each string stretched from the quark of one baryon to the diquark of the other, Fig. 2a. A baryon-antibaryon collision would give one string between a quark and an antiquark and another one between a diquark and an antidiquark, Fig. 2b.

It remains to be specified how the two strings should share the available energy. Following [24] one may e.g. choose an ansatz

$$P(\chi) = \frac{(1-\chi)^2}{(\chi^2 + c^2)^{1/4}} \tag{16}$$

for the fraction χ that the quark takes of the baryon energy, with $1 - \chi$ taken by the diquark. The cutoff $c = 2m_q/s^{1/2} \approx 0.6\ \mathrm{GeV}/s^{1/2}$ is not really necessary here, but is included for further reference.

If an event contains a hard interaction, the string drawing issues become more complicated, since there may be many ways of connecting the colour charges of the outgoing objects. Furthermore, the standard QCD cross-sections cannot be uniquely split into a sum of terms, where each term corresponds to a well defined colour flow, since also interference terms are present. These

interference terms are suppressed by $1/N_C^2$, where $N_C = 3$ is the number of colours. By neglecting the interference terms, it is possible to obtain a consistent scheme for selecting the string drawing in a given event [26]. One possible string drawing for $gg \to gg$ scattering is shown in Fig. 2c. This string drawing, as well as all other one-gluon exchange processes between gluons and valence quarks, reduce to the simple low-p_T two-string picture when the p_T of the hard scattering vanishes.

When several hard scatterings are present in an event, string drawing issues become even more complicated. Specifically, the string drawing now depends on the relative colour arrangement, in each hadron individually, of the partons that are about to scatter. This is a subject about which nothing is known. Many scenarios could therefore be envisioned. The simplest is to assume that, following the hardest interaction, all subsequent ones are of the $gg \to gg$ type, with the two gluons in a colour singlet state. Then each interaction will result in a double string being stretched directly between the two outgoing gluons, decoupled from the rest of the system. Only the hardest interaction gives strings coupled to the beam remnants. This is the solution adopted for the moment, with further alternatives to be discussed in section 4.5. While details are sensitive to the choice made, the overall picture is surprisingly stable, as will be shown later.

With the energy of scattered partons subtracted, eq. (16) could still be used to give the sharing of remaining energy between the quark and the diquark. If several interactions are to be allowed per event, this tends to lead to a too high average charged multiplicity, so in the multiple interaction scenario eq. (16) is replaced by the structure function inspired

$$P(\chi) = \frac{(1-\chi)^3}{(\chi^2 + c^2)^{1/2}} \tag{17}$$

throughout.

A hard interaction between coloured objects is, by necessity, associated with the possibility of having initial and final state radiation. For technical reasons, this is here included only for the hardest interaction. In practice, there is no problem: except for the hardest interaction, which can be hard because of experimental trigger conditions, it is unlikely for a parton scattering to be so hard that radiation plays a significant rôle. The final state radiation formalism used is the one presented in [27], including coherence effects [28], while initial state radiation is described with the

help of the "backwards evolution" formalism developed in [29]. In the context of the leading log type parton showers thus described, the string drawing is straightforward.

Given a set of outgoing coloured partons, with information about how these partons are connected via strings, the Lund string fragmentation model [30] provides a description of the subsequent hadronization. In its Monte Carlo implementation [4], the developments in [31] are of vital importance, including as they do the treatment of very complicated partonic states, where some string pieces may also have rather small invariant masses.

3. Results with No Impact Parameter Dependence

In this section we wish to give a brief review of the shortcomings of some simple models for hadronic events, with and without multiple interactions. This will provide the incentive for introducing an impact parameter picture in the next section.

3.1. The Simple Two-String Picture

The simplest possible model for hadronic events is the two-string picture described in section 2.3. There are no hard interactions at all, and the only degrees of freedom are the two χ variables, which determine the masses of the two string systems.

In Fig. 3 this model is compared with the UA5 acceptance-corrected data on the charged multiplicity distribution for 540 GeV $p\bar{p}$ events [32]. It is immediately noted that the model gives far too narrow a distribution. This is basically the statement that multiplicity distributions in e^+e^- annihilation are much more narrow than in hadron physics. Comparing the two-string hadronic events with the e^+e^- one-string ones, the fluctuation of string masses in the former does broaden the distribution, but nowhere near enough.

Another interesting observable is the forward-backward correlation, defined in the following way. Consider two bins in pseudorapidity, one between $\Delta\eta/2$ and $\Delta\eta/2 + 1$ (forward), the other between $-\Delta\eta/2$ and $-(\Delta\eta/2 + 1)$ (backward), i.e. two one unit wide bins separated by a central gap of $\Delta\eta$. Call the charged multiplicities in the two bins n_F and n_B, and define the correlation

coefficient by

$$b = \frac{\langle n_F n_B\rangle - \langle n_F\rangle^2}{\langle n_F^2\rangle - \langle n_F\rangle^2} \tag{18}$$

(for $\langle n_B\rangle = \langle n_F\rangle$ and $\langle n_B^2\rangle = \langle n_F^2\rangle$). In Fig. 4 the correlation coefficient b is plotted as a function of $\Delta\eta$, again comparing the model with UA5 data [33]. Apart from a very small short-range effect, the model does not predict any forward-backward correlations.

3.2. Introduction of Hard Interactions

A model that only contains partons with small transverse momenta is obviously a simplification. With a sharp cutoff of the perturbative two-jet cross-section at p_{Tmin} = 1.8 GeV, roughly two thirds of all events would be expected to contain a hard interaction. The remaining 1/3 is still assumed to be low-p_T.

The inclusion of hard interactions actually results in negligible improvements of Figs. 3 and 4. The reason is that most "hard" interactions still have a p_T for the scattered partons in the range 2 - 3 GeV, i.e. not enough to make a difference in the event structure.

If initial and final state radiation effects are included, some further improvements are noted in Figs. 3 and 4. Again the soft nature of most interactions make the effect less than adequate, however.

Whereas some uncertainty may be present in the details of what is included up to this point, even rather drastic variations are insufficient to come anywhere near an explanation of the data.

3.3. Effects of Multiple Interactions

Multiple interactions are now introduced above some given p_{Tmin} scale, using the formalism explained in section 2.2. Events which do not give any interactions above p_{Tmin} are again classified as two-string low-p_T events.

There is thus one main free parameter in the problem, p_{Tmin}. As p_{Tmin} is decreased, the average number of interactions is increased, and so are the fluctuations in this number. Events which contain a large number of interactions also have large multiplicities. In Fig. 5 it is shown how the multiplicity distribution evolves as p_{Tmin} is decreased from 2.0 to 1.6 to 1.2 GeV. At the same time, the average number of interactions per event is increased from 0.56 to 1.01 to 2.11. A fair agreement with the high-multiplicity tail is obtained for p_{Tmin} = 1.6 GeV. With an energy sharing between diquark and quark given by eq. (17), the $\langle n_{ch}\rangle$ values go from 29 to 33 to 42. Compared with the UA5 figure of $\langle n_{ch}\rangle \approx 29$ [32], only the first two p_{Tmin} values are acceptable. If instead the energy sharing is given by eq. (16), corresponding to a higher $\langle n_{ch}\rangle$ before any hard interactions at all are introduced, only the higher p_{Tmin} value would give an acceptable $\langle n_{ch}\rangle$, but then without reproducing the high multiplicity tail.

With multiple interactions included, the forward-backward correlations are of significant size, Fig. 6, since the number of scatterings strongly influences the multiplicity in both hemispheres simultaneously. Also several other observations, e.g. the rate of "hot spots" [34], are now understood.

There are other places where this scenario fails, however. One is that it underestimates the energy away from the core of a jet, Fig. 7, i.e. there is not a large enough "pedestal effect" in the model. This would seem to imply that events containing one hard interaction also contain an above-average amount of extra semihard interactions, i.e. effects of varying impact parameters.

4. The Model with Variable Impact Parameters

Up to this point, it has been assumed that the initial state is the same for all hadron collisions, whereas in fact each collision also is characterized by a varying impact parameter b. Within the classical framework of this paper, b is to be thought of as a distance of closest approach, not as the Fourier transform of the momentum transfer. A small b value corresponds to a large overlap between the two colliding hadrons, and hence an enhanced probability for multiple interactions. A large b, on the other hand, corresponds to a grazing collision, with a large probability that no parton-parton interactions at all take place.

4.1. The Hadronic Matter Distribution

In order to quantify the concept of hadronic matter overlap, one may assume a spherically symmetric distribution of matter inside the hadron, $\rho(\bar{x})\ d^3x = \rho(r)\ d^3x$. For simplicity, the same spatial distribution is taken to apply for all parton species and momenta. Four different parametrizations of the matter distribution have been compared, to check how sensitive results are to this choice. The first three are a solid sphere $\rho_1(r) \propto \theta(a-r)$, a Gaussian $\rho_2(r) \propto \exp(-r^2/a^2)$ and an exponential $\rho_3(r) \propto \exp(-r/a)$. Since differences in physics results between these three turned out to be smaller than anticipated, and since none of them gave a sufficiently large pedestal effect, the fourth possibility was chosen to be a double Gaussian

$$\rho_4(r) \propto (1-\beta)\ \frac{1}{a_1^3}\exp(-\frac{r^2}{a_1^2}) + \beta\ \frac{1}{a_2^3}\exp(-\frac{r^2}{a_2^2}). \tag{19}$$

This corresponds to a distribution with a small core region, of radius a_2 and containing a fraction β of the total hadronic matter, embedded in a larger hadron of radius a_1. While it is mathematically convenient to have the origin of the two Gaussians coinciding, the physics could well correspond to having three disjoint core regions, reflecting the presence of three valence quarks, together carrying the fraction β. One could alternatively imagine a hard hadronic core surrounded by a pion cloud, as in the chiral bag model [36]. To be specific, the values $\beta = 0.5$ and $a_1/a_2 = 5$ have been used throughout this paper. The double Gaussian will be used as the standard matter distribution in the following. It should be noted that the overall distance scale a (or a_1) never enters in the subsequent calculations, since the inelastic, nondiffractive cross-section $\sigma_{nd}(s)$ is taken from literature rather than calculated from the $\rho(r)$.

For a collision with impact parameter b, the time-integrated overlap between the matter distributions of the colliding hadrons is given by

$$\ddot{O}(b) = \iint d^3x\ dt\ \rho_{boosted}(x-\frac{b}{2},\ y,\ z-vt)\ \rho_{boosted}(x+\frac{b}{2},\ y,\ z+vt), \tag{20}$$

where v is the velocity in the CM frame and $\rho_{boosted}$ the suitably Lorentz contracted $\rho(\bar{x})$. By a scale change in z, $\rho_{boosted}$ can be replaced by ρ. After a further scale change in t one obtains

$$\begin{aligned}\ddot{O}(b) &\propto \iint d^3x\ dt\ \rho(x-\frac{b}{2},\ y,\ z-\frac{t}{2})\ \rho(x+\frac{b}{2},\ y,\ z+\frac{t}{2}) = \\ &= \int dt \int d^3x\ \rho(x,\ y,\ z)\ \rho(x,\ y,\ z-(b^2+t^2)^{1/2}).\end{aligned} \tag{21}$$

As an example, the double Gaussian of eq. (19) gives

$$\tilde{O}_4(b) \propto (1-\beta)^2 \frac{1}{2a_1^2} \exp\{-\frac{b^2}{2a_1^2}\} + 2\beta(1-\beta) \frac{1}{a_1^2+a_2^2} \exp\{-\frac{b^2}{a_1^2+a_2^2}\} + \\ + \beta^2 \frac{1}{2a_2^2} \exp\{-\frac{b^2}{2a_2^2}\}. \tag{22}$$

In addition to the $\tilde{O}(b)$ obtained with the $\rho_1 - \rho_4$ above, it is useful to have an alternative $\tilde{O}_0(b) \propto \theta(a-b)$, i.e. where all events have the same overlap. This may be thought of as collisions at an average, fixed impact parameter. It will not be exactly equivalent to the formalism of section 2, for reasons that will become apparent.

The overlap $\tilde{O}(b)$ is obviously strongly related to the eikonal $\Omega(b)$ of optical models. We have kept a separate notation, since the physics context of the two is slightly different: $\Omega(b)$ is based on the quantum mechanical scattering of waves in a potential, and is normally used to describe the elastic scattering of a hadron-as-a-whole, while $\tilde{O}(b)$ comes from a purely classical picture of pointlike partons distributed inside the two colliding hadrons. Furthermore, the normalization and energy dependence is differently realized in the two formalisms.

4.2. The Variable Impact Parameter Formalism

The larger the overlap $\tilde{O}(b)$ is, the more likely it is to have interactions between partons in the two colliding hadrons. In fact, there should be a linear relationship

$$\langle\tilde{n}(b)\rangle = k\tilde{O}(b) \tag{23}$$

where $\tilde{n} = 0, 1, 2, 3, \ldots$ counts the number of interactions when two hadrons pass each other with an impact parameter b. The constant of proportionality, k, is related to the parton-parton cross-section and hence increases with CM energy.

For each given impact parameter, the number of interactions is assumed to be distributed according to a Poissonian. If the matter distribution has a tail to infinity (which is true for the examples above, except for the solid sphere), events may be obtained with arbitrarily large b values. In order to

obtain finite total cross-sections, it is necessary to assume that each event contains at least one semihard interaction. The probability that two hadrons, passing each other with an impact parameter b, will actually undergo a collision is then given by

$$P_{int}(b) = 1 - e^{-\langle\tilde{n}(b)\rangle} = 1 - e^{-k\tilde{O}(b)} \tag{24}$$

according to Poissonian statistics. The average number of interactions per event at impact parameter b is now

$$\langle n(b)\rangle = \frac{\langle\tilde{n}(b)\rangle}{P_{int}(b)} = \frac{k\tilde{O}(b)}{1 - \exp(-k\tilde{O}(b))}, \tag{25}$$

where the denominator comes from the removal of hadrons which passed without colliding, i.e. with $\tilde{n} = 0$.

In section 2, the relationship $\langle n\rangle = \sigma_{hard}/\sigma_{nd}$ was introduced for the average number of interactions per nondiffractive, inelastic event. When averaged over all impact parameters, this relation must still hold true: the introduction of variable impact parameters may give more interactions in some events and less in others, but it does not affect either σ_{hard} or σ_{nd}. For the former this is because the perturbative QCD calculations only depend on the total parton flux, for the latter by construction. Integrating eq. (25) over b one then obtains

$$\langle n\rangle = \frac{\int \langle n(b)\rangle P_{int}(b)\, d^2b}{\int P_{int}(b)\, d^2b} = \frac{\int k\tilde{O}(b)\, d^2b}{\int (1 - \exp(-k\tilde{O}(b)))\, d^2b} = \frac{\sigma_{hard}}{\sigma_{nd}}. \tag{26}$$

For $\tilde{O}(b)$, σ_{hard} and σ_{nd} given, with $\sigma_{hard}/\sigma_{nd} > 1$, k can thus always be found (numerically) by solving the last equality.

The absolute normalization of $\tilde{O}(b)$ is not interesting in itself, but only the relative variation with impact parameter. It is therefore useful to introduce an "enhancement factor" $f(b)$, which gauges how the interaction probability for a passage with impact parameter b compares with the average, i.e.

$$\langle\tilde{n}(b)\rangle = k\tilde{O}(b) = f(b)\, \langle k\tilde{O}\rangle. \tag{27}$$

In other words,

$$f(b) = \frac{\tilde{O}(b)}{\langle\tilde{O}\rangle} = \frac{\langle\tilde{n}(b)\rangle}{\langle\tilde{n}\rangle}. \tag{28}$$

The definition of the mean $\langle\tilde{O}\rangle$ is not unambiguous. With the choice to let $\langle\tilde{O}\rangle$

be the average of all events, i.e. where $\tilde{n} \geqslant 1$,

$$\langle \tilde{O} \rangle = \frac{\int \tilde{O}(b)\, P_{int}(b)\, d^2b}{\int P_{int}(b)\, d^2b}, \tag{29}$$

one obtains

$$\langle f \rangle = \frac{\int f(b)\, P_{int}(b)\, d^2b}{\int P_{int}(b)\, d^2b} = \frac{\int \tilde{O}(b)\, P_{int}(b)\, d^2b}{\langle \tilde{O} \rangle \int P_{int}(b)\, d^2b} = 1, \tag{30}$$

i.e. the average value of $f(b)$ over all events is unity. A large f value corresponds to a high probability for several interactions, while a small f corresponds to a peripheral collision with the minimal number of one interaction. The larger a tail the hadronic matter distribution has, or the more peaked it is at the origin, the wider the probability distribution in f is.

A further number needed in the following is

$$f_c = \frac{\int \tilde{O}(b)\, P_{int}(b)\, d^2b}{\int \tilde{O}(b)\, d^2b}, \tag{31}$$

which is impact parameter independent. Typically f_c is somewhat smaller than one, approaching unity from below when $\sigma_{hard}/\sigma_{nd} \to \infty$. The function of f_c will be to compensate for the fact that the average number of interactions per event is pushed up by the requirement that each event contain at least one interaction.

If eqs. (27), (29), (31) and (26) are combined, one obtains

$$\begin{aligned} \langle \tilde{n}(b) \rangle &= f(b)\, \langle k\tilde{O} \rangle = f(b) \frac{\int k\tilde{O}(b)\, P_{int}(b)\, d^2b}{\int P_{int}(b)\, d^2b} = \\ &= f_c f(b) \frac{\int k\tilde{O}(b)\, d^2b}{\int P_{int}(b)\, d^2b} = f_c f(b) \frac{\sigma_{hard}}{\sigma_{nd}}. \end{aligned} \tag{32}$$

This derivation, which has been given here for the total number of interactions for two hadrons passing each other at an impact parameter b, could equally well have been carried out for the number of interactions in a given p_T bin (since, contrary to the case of $n(b)$, there is no constraint of the type $\tilde{n}(b) \geqslant 1$). The conclusion is therefore that the effective probability $p(x_T)$ of eq. (6), giving the probability of having a scattering at x_T, should

be replaced by

$$p(x_T, b) = f_c f(b)\, p(x_T) = f_c f(b) \frac{1}{\sigma_{nd}} \frac{d\sigma}{dx_T}. \tag{33}$$

The naive generation procedure is thus to pick a b according to the phase space d^2b, find the relevant $f(b)$ and plug in the resulting $p(x_T, b)$ in the formalism of section 2.2. If at least one hard interaction is generated, the event is retained, else a new b is to be found. This algorithm would work fine for hadronic matter distributions which vanish outside some radius, so that the d^2b phase space which needs to be probed is finite. Since this is not true for the distributions under study, it is necessary to do better.

4.3. The Event Generation Formalism

By analogy with eq. (7), it is possible to ask what the probability is to find the hardest scattering of an event at x_{T1}. For each impact parameter separately, the probability to have an interaction at x_{T1} is given by $p(x_{T1}, b)$ in eq. (33), and this should be multiplied by the probability that the event contains no interactions at a scale $x_T' > x_{T1}$, to yield the total probability distribution

$$\frac{dP_{hardest}}{d^2b\, dx_{T1}} = p(x_{T1}, b) \exp\left\{-\int_{x_{T1}}^{1} p(x_T', b)\, dx_T'\right\}. \tag{34}$$

There are two ways to proceed from this formula. One is to integrate eq. (34) over all allowed x_T values, to give the probability that a passage produces at least one interaction

$$\begin{aligned} \frac{dP_{\geqslant 1}}{d^2b} &= \int_{x_{Tmin}}^{1} dx_T\, p(x_T, b) \exp\left\{-\int_{x_T}^{1} p(x_T', b)\, dx_T'\right\} = 1 - \exp\left\{-\int_{x_{Tmin}}^{1} p(x_T', b)\, dx_T'\right\} = \\ &= 1 - \exp\left\{-f_c f(b) \frac{\sigma_{hard}}{\sigma_{nd}}\right\} = 1 - \exp(-k\tilde{O}(b)) = P_{int}(b), \end{aligned} \tag{35}$$

in agreement with eq. (24). A proper procedure would therefore be to select a b according to $P_{int}(b)\, d^2b$. This yields the $f(b)$ value and hence the relevant $p(x_T, b)$. The $p(x_T, b)$ can be directly plugged into the formalism of section 2.2, to yield a sequence of x_{Ti} values for interactions. If no x_T values at all are found above x_{Tmin}, which happens with probability $\exp(-k\tilde{O}(b))$, the interaction generation chain is to be restarted at $x_{T0} = 1$, until a valid event (with $\geqslant 1$ interaction) is found.

The procedure above is straightforward to implement, but it suffers from the disadvantage that it is only relevant for the generation of the inclusive sample of nondiffractive, inelastic events. In particular, it cannot be used to generate the activity accompanying a high-p_T jet or a W, say, since such events are not distributed according to $P_{int}(b)$, but rather are biased towards smaller b values. The following trick can then be used.

If the treatment of the exponential in eq. (34) is deferred for a moment, the equation reads

$$\frac{dP_{hardest}}{d^2b\ dx_{T1}} = p(x_{T1},b) = f_c f(b)\ \frac{1}{\sigma_{nd}}\ \frac{d\sigma}{dx_T}(x_{T1}). \tag{36}$$

Here the distribution in b and x_{T1} appears in factorized form, so that the two can be chosen independently of each other. In particular, a high-p_T jet or W can be chosen with whatever kinematics desired. For a W (or any s-channel resonance) there would be no obvious x_T scale by itself but, since x_T is used as a measure of the hardness of an interaction, a choice $x_T^2 \approx \tau = \hat{s}/s$ is not unreasonable. With the b chosen according to $f(b)\ d^2b$, the neglected exponential

$$\exp\{-\int_{x_{T1}}^{1} p(x_T',b)\ dx_T'\} = \exp\{-\ f_c f(b) \int_{x_{T1}}^{1} p(x_T')\ dx_T'\} \tag{37}$$

can now be evaluated, and the event retained with a probability proportional to it. From the x_T scale of the selected interaction, a sequence of softer x_{Ti} values may again be generated as in section 2.2, using the known $p(x_T,b)$. This sequence may be empty, i.e. the event need not contain any further interactions.

It is interesting to understand how the algorithm above works. By selecting b according to $f(b)\ d^2b$, i.e. $\delta(b)\ d^2b$, the primary b distribution is maximally biased towards small impact parameters. If the first interaction is hard, by choice or by chance, the integral of the cross-section above x_{T1} is small, and the exponential in eq. (37) close to unity. Almost all events are therefore retained. The large $f(b)$ value is also likely to lead to the generation of many further, softer interactions. If, on the other hand, the first interaction is not hard, the exponential is no longer close to unity, and many events are rejected. Since the exponent in eq. (37) is proportional to $f(b)$, a large $f(b)$ leads to an enhanced probability for rejection, whereas the chance of acceptance is larger with a small $f(b)$. Among events where the hardest

interaction is soft, the b distribution is therefore biased towards larger values (smaller $f(b)$), and there is a small probability for yet softer interactions.

4.4. Cross-Section Considerations

In this section, nothing has yet been assumed about the form of the $d\sigma/dp_T$ spectrum. Like in the impact parameter independent case, it is possible to use a sharp cutoff at some given p_{Tmin} value. However, here each event is required to have at least one interaction, whereas before events without interactions were retained and put at $p_T = 0$. It is therefore aesthetically more appealing to assume a more gradual turnoff, so that a (semi)hard interaction can be rather soft part of the time. The matrix elements roughly diverge like $\alpha_s^2(p_T^2)\cdot dp_T^2/p_T^4$ for $p_T \to 0$. They could therefore be regularized as follows. Firstly, to remove the $1/p_T^4$ behaviour, multiply by a factor $p_T^4/(p_{T0}^2+p_T^2)^2$. Secondly, replace the p_T^2 argument in α_s by $p_{T0}^2+p_T^2$ or, with the inclusion of the K-factor introduced in section 2.1, replace $0.075\cdot p_T^2$ by $0.075\cdot(p_{T0}^2+p_T^2)$.

With these substitutions, a continuous p_T spectrum is obtained, stretching from $p_T = 0$ to $s^{1/2}/2$. For $p_T \gg p_{T0}$ the standard perturbative QCD cross-section is recovered, while values $p_T \ll p_{T0}$ are strongly damped. The p_{T0} scale, which now is the main free parameter of the model, in practice comes out to be of the same order of magnitude as p_{Tmin} did, i.e. roughly 2 GeV.

If gluons with large transverse wavelength decouple because of the colour singlet nature of hadrons, and if the transverse structure of hadrons is assumed to be energy-independent, it is natural to assume that also p_{Tmin} and p_{T0} are independent of the CM energy of the hadron collision. For the impact parameter independent picture this works out fine, with all events being reduced to low-p_T two-string ones when the CM energy is reduced. In the variable impact parameter picture, the whole formalism only makes sense if $\sigma_{hard} > \sigma_{nd}$, see e.g. eq. (26). Since σ_{nd} does not vanish with decreasing energy, but σ_{hard} would do that for a fixed p_{T0}, this means that p_{T0} has to be reduced when the energy is decreased.

It is reasonable to ask how meaningful the whole physics scenario becomes at small CM energies. The picture of multiple parton-parton interactions is certainly easier to visualize as a high-energy behaviour, and as involving parton scatterings typically with a few GeV of transverse momentum. In the

description of events at lower energies, where more emphasis would have to be put on interactions at small p_T values, the picture loses some of its lustre. Possibly a physics description in other terms would be more sensible here - although the correct answer is unique, different approximations may do more or less well in a given region. Keeping this warning in mind, it is still meaningful to see what happens as the energy is varied.

Going a bit ahead of the story, the p_{T0} values at a given CM energy can be determined "simply" by the requirement that the mean charged multiplicity in the model should agree with the experimental one. Typical values obtained that way (with an uncertainty not only due to experimental errors, but also in the understanding of the relevant trigger conditions to use for Monte Carlo comparisons) are shown in Fig. 8 as a function of CM energy for the double Gaussian matter distribution. The increase of p_{T0} with energy is fairly slow, particularly for the higher energies. In the Sp$\bar{p}$S energy range, a logarithmic fit would give

$$p_{T0} = 2.0 \text{ GeV} + 0.08 \text{ GeV} \cdot \ln\left(\frac{s^{1/2}}{540 \text{ GeV}}\right) \tag{38}$$

If anything, an extrapolation of this trend would probably overestimate the p_{T0} at higher values. Taking the value at 540 GeV as a lower limit, this would suggest $2.0 < p_{T0} < 2.35$ at 40 TeV. Although the variation of p_{T0} with energy in eq. (38) is slow, the effect on the average number of interactions per event is rather drastic, leading to a considerably slower increase than is obtained with a fix p_{T0}, Fig. 9.

While predicting cross-sections is in no way the objective of this paper, it could still be interesting to see what the p_{T0} values determined above correspond to in terms of the inelastic, nondiffractive cross-section σ_{nd}. Since no explicit scales have been introduced for the hadronic matter distribution, the absolute normalization is not known, but the energy dependence can be studied. In Fig. 10 the integral $\int P_{int}(b)\, d^2b$ is shown, normalized to the parametrized σ_{nd} at 540 GeV. By and large, agreement with the parametrization is not that bad at higher energies, which at least shows that the model has some sense of internal consistency. The results at small energies are fairly unreliable: the multiplicity distribution is here more sensitive to variations in the string drawing algorithm (specifically, to the method used for the hardest interaction) than to changes of p_{T0}. Further, no systematic attempt has been made to study and correctly include the small differences in behaviour between pp and p$\bar{p}$ events.

4.5. String Drawing Issues

In section 2.3, a description was given of one possible way of assigning flavours to and drawing strings between the scattered partons. In general, this formalism is retained. A few modifications have been introduced, however, as described in the following. It is not obvious a priori whether these are improvements or not, but this reflects the major uncertainties in this game.

With the introduction of a soft regularization of the cross-section at $p_T = 0$, many events come to contain a hardest interaction with a p_T in the region 0 - 1 GeV, i.e. fairly soft. Standard structure function parametrizations typically extend down to some Q_0 scale in the order of 2 GeV. The normal procedure, to use the structure function values at Q_0 whenever $p_T \leq Q_0$, may give an erroneous picture of the hadron at small Q^2 scales. Specifically, it leads to a dominance of gluon-gluon scatterings over gluon-quark or quark-quark ones, whereas a not unreasonable scenario would have the valence quarks dominate the low-Q^2 hadron. We have therefore tried a simple recipe for enhancing the valence quark content of the hadron at small p_T, as follows. With kinematics for the interaction chosen, a fraction $p_{T0}^2/(p_{T0}^2+p_T^2)$ of the events is reassigned to correspond to a scattering between two valence quarks of the two incoming hadrons, while for the remaining fraction $p_T^2/(p_{T0}^2+p_T^2)$, flavours are chosen as usual. The kinematics of the hard interaction therefore replaces the selection of two χ variables for most interactions at small p_T values.

In section 2.3, it was assumed that all interactions after the hardest one were gluon-gluon scatterings, with the two gluons in a colour singlet state. Here a more realistic mix is introduced. One third of all non-hardest interactions is assumed to be of the two-gluon type above, and an additional one third is taken to give a string stretched between a q$\bar{q}$ pair (q = u, d or s). The final 1/3 is again gluon-gluon scatterings, but here colour correlations are assumed such that each of the gluons should be connected unto one of the strings "already" present. Among the different possibilities of connecting the colours of the gluon, the one which minimizes the total increase in string length will be chosen. This is in contrast to the gluon-gluon closed loop alternative, which roughly corresponds to a maximization of the extra string length. The three alternatives are illustrated in Fig. 11.

Sadly absent in the list above is the possibility that several of the valence quarks of the incoming hadrons interact independently of each other. While the scattering of one valence quark out of the baryon leaves a colour antitriplet diquark beam remnant carrying the baryon number, the scattering of a second valence quark is likely to set the baryon number in transverse motion. One simple scenario for this is to assume that the baryon is a Y-shaped string configuration, with a quark at each endpoint and the baryon number effectively associated with the junction point. If the ends are set in motion or re-attached by gluon exchanges, the junction point will start moving in a well-defined fashion [37] so as to minimize the total string length. As the three legs of the Y-shaped string starts fragmenting, the baryon is going to be the one created around the junction. Without invoking any kind of "hard diquark scattering" mechanism [38], this could well explain the abnormal rate of baryons at medium high p_T observed experimentally [39]. Unfortunately there is a catch: the fragmentation of a Y-shaped string is extremely difficult to handle in a consistent manner, and the problem has never been solved. We hope to return to this issue, and to a more realistic flavour composition of the non-hardest interactions, at a later date.

For the main features of events, like the ones studied in this paper, the effects of the uncertainties involved should probably not be overemphasized. Whereas the three components above are usually evenly mixed, it is possible to study what happens if only one is used. Since the three represents different extremes, with the truth probably somewhere in between, it is comforting to note that a fair description of the data (but with different p_{T0} cutoffs) can be obtained with either of the three extreme possibilities.

In the multiplicity distributions shown in section 3, one of the problems always was that the model did not produce enough low-multiplicity events. Whereas the UA5 trigger conditions remove almost all single diffractive events, most double diffractive ones survive and are included in the multiplicity distributions. In the following, the generation of diffractive events has therefore been included where relevant. This is made according to a simple model, with a dM^2/M^2 spectrum for the mass of each diffractive system. Each system is represented by a string stretched between a diquark in the forward end and a quark in the other one. Except for some tries with a double string stretched from a diquark and a quark in the forward direction to a central gluon, which gave only modest changes in the results, no attempts have been made with more detailed models for diffractive states [40].

5. Multiplicity Distributions

The charged multiplicity distribution is interesting, despite its deceptive simplicity, since most physical mechanisms (of those playing a rôle in minimum bias events) contribute to the multiplicity buildup. This was illustrated in section 3. From now on we will use the complete model, i.e. including multiple interactions and varying impact parameters, to look more closely at the data. Single and double diffractive events are now also included; with the UA5 triggering conditions roughly 3/4 of the generated double diffractive events are retained, while the contribution from single diffraction is negligible.

5.1. Total Multiplicities

A final comparison with the UA5 data at 540 GeV is presented in Fig. 12, for the double Gaussian matter distribution. The agreement is now generally good, although the value at the peak is still a bit high. In this distribution, the varying impact parameters do not play a major rôle; for comparison, Fig. 12 also includes the other extreme of a fix overlap $\tilde{O}_0(b)$ (with the use of the formalism in section 4, i.e. requiring at least one semihard interaction per event, so as to minimize other differences). The three other matter distributions, solid sphere, Gaussian and exponential, are in between, and are all compatible with the data.

Within the model, the total multiplicity distribution can be separated into the contribution from (double) diffractive events, events with one interaction, events with two interactions, and so on, Fig. 13. While 45% of all events contain one interaction, the low-multiplicity tail is dominated by double diffractive events and the high-multiplicity one by events with several interactions. The average charged multiplicity increases with the number of interactions, Fig. 14, but not proportionally: each additional interaction gives a smaller contribution than the preceding one. This is partly because of energy-momentum conservation effects, and partly because the additional "messing up" when new string pieces are added has less effect when many strings already are present. The same phenomenon is displayed in Fig. 15, here as a function of the "enhancement factor" $f(b)$, i.e. for increasingly central collisions.

The multiplicity distributions for the 200 and 900 GeV UA5 data have not been published, but the moments have [41], and a comparison with these is presented in Table 1. The $\langle n_{ch} \rangle$ value was brought in reasonable agreement with the data, at each energy separately, by a variation of the p_{T0} scale. The moments thus obtained are in reasonable agreement with the data.

5.2. Energy Dependence

Extrapolating to higher energies, the evolution of average charged multiplicity with energy is shown in Fig. 16. The results do depend on the choice of p_{T0} value, but not crucially so. In addition, the assumptions about flavours and string drawing between scattered partons can be varied to give an even wider band of possible $\langle n_{ch} \rangle$ at higher energies. The dependence of $\langle n_{ch} \rangle$ on the number of interactions in the event is shown also for higher energies in Fig. 14, and the dependence on the "enhancement factor" $f(b)$ is shown in Fig. 15.

The multiplicity distributions themselves are shown in Fig. 17, for 1.6, 5, 15 and 40 TeV CM energy, to exemplify the typical shape predicted. The differences that come from the choice of matter distribution are illustrated at 40 TeV in Fig. 18. Contrary to results at $Sp\bar{p}S$, the dependence on this choice is now appreciable. Thus the distributions for a solid sphere, a Gaussian or an exponential all are narrower than for the 540 GeV data, while the double Gaussian produces a much broader shape.

It is interesting to take the ratio $D/\langle n \rangle$, the dispersion over the mean, as a measure of the width, and study how the energy variation changes when pieces of physics are added on, Fig. 19. If hadronic events only consisted of one string, spanned between the two outgoing hadron remnants, the multiplicity distribution would be essentially Poissonian, and $D/\langle n \rangle$ would decrease monotonically with increasing energy. A minimal model for low-p_T events should probably be based on a two-string model, however. Then the sharing of beam remnant energy would lead to varying invariant masses for the two string pieces, a variation which is enough to understand why $D/\langle n \rangle$ does not decrease in the fixed target energy range. (The higher $D/\langle n \rangle$ value for the one-string model at low energies is due to a lower average multiplicity than in the two-string model or in the data, and the dispersion itself is everywhere smaller with one than with two strings.) At ISR energies, this variation would not suffice, but here hard interactions (including associated initial and final

state radiation) start to play a rôle. The effect of having just one interaction is not large, however, and it is only when a varying number of interactions is included that a reasonable description is obtained at $Sp\bar{p}S$ energies. If no variation in impact parameter is included, the distribution in number of interactions is again Poissonian, and thus with a relative width that decreases as the average number increases. In fact, the scaled multiplicity distribution would reach its maximum width already at around 1 TeV, in contradiction with the trend of the UA5 data. It is therefore necessary to introduce the variable impact parameter picture. The distribution in impact parameter b, and hence enhancement factor f, is not governed by Poissonian statistics. Specifically, if the mean number of interactions per event increases with energy, then so does the width of the f distribution. It is only this step that ensures a non-shrinking multiplicity distribution at higher energies. (The funny bump in $D/\langle n \rangle$ that appears at around 50 GeV is strongly related to the assumptions about the string drawing for the hardest interaction, sections 4.4 and 4.5, and should not be taken too seriously.) Finally, the inclusion of double diffractive events is a separate issue in our scenario, but one that is needed to understand the low-multiplicity region. It also contributes to the $D/\langle n \rangle$ ratio measured by experiments.

In our model there is nothing natural about the approximate KNO scaling [42] observed at lower energies: with the exception of the variable impact parameters, each piece of physics by itself would asymptotically give a shrinking distribution. There is therefore no support for the validity of "two-component" scenarios [43], in which minijet events with a higher $\langle n_{ch} \rangle$ are added on to an immutable low-p_T event KNO distribution.

The DTU-type models [8-11] provide an explanation for the shape of the multiplicity distribution akin to ours. In addition, a number of theoretical models exist in which a simple underlying principle is sought (a few of these are found in [44]). Such models, which often lead to negative binomial type multiplicity distributions, are very successful in explaining multiplicity phenomena. There is also an economy of parameters which contrasts markedly to the complex scenario outlined in this paper. However, it remains to be seen if the present simplicity can be maintained when these models are extended to cover all particle production phenomena at hadron colliders, as our model in principle attempts to do.

5.3. Multiplicity in Pseudorapidity Bins

The inclusive pseudorapidity distribution at 200, 540 and 900 GeV is compared with UA5 data [45] in Fig. 20. In fact, the p_{T0} scales determined from the average total multiplicity had to be lowered by roughly 0.1 GeV in order to achieve the agreement observed; without it the curves would have been below the data almost everywhere. The change corresponds to an increase in the total charged multiplicity at 540 GeV roughly from 29 to 31. It is possible that this comes from differences between our model and UA5:s extrapolations in the region $|\eta| > 5$. Note that the dip at $\eta = 0$ is entirely kinematical: had true rapidity been used instead, there would have been no dip. The pseudorapidity distribution for different multiplicity bins is displayed in Fig. 21. Generally the agreement is satisfactory, but in the low-multiplicity bins we predict a much deeper central dip than observed experimentally. This probably indicates that our diffractive model is not entirely satisfactory. One possibility would be to introduce a component of central diffraction at the expense of double diffraction. Here experimental studies could be of help: are the particles in a given low-multiplicity event still fairly evenly distributed in η, or are they concentrated in a smaller region, the position of which varies from event to event?

The comparison with scaled multiplicity distributions in rapidity bins, Fig. 22, shows fair agreement with the UA5 data [47], but with a tendency to overestimate fluctuations.

Forward-backward multiplicity correlations are again shown in Fig. 23, compared with the UA5 results. It now seems we have somewhat stronger correlations than the data, but it is not incompatible. To some extent, the amount of fluctuations and correlations could be "fine-tuned" by a variation of the details of the string-drawing, sect. 4.5.

6. Transverse Momentum Properties and Jets

The multiplicity distribution is mainly influenced by longitudinal fragmentation properties. For the transverse momentum properties, contributions are obtained from the fragmentation of simple strings, and from high-p_T jet production with associated initial and final state radiation. These add no new degrees of freedom, but are completely specified by the properties of the model and by our knowledge of e^+e^- annihilation

phenomenology. The only nontrivial input given was to use $\alpha_s(0.075 \cdot p_T^2)$ for the hard interaction; an effective K-factor ≈ 1.5 or a $\Lambda \approx 0.7$ GeV (rather than the 0.2 GeV used) would have done as well. It is therefore here that the model can be checked.

Since the comparisons presented elsewhere are made without reference to the particle species involved, Fig. 24 serves as a reminder that the model actually also contains predictions for the flavour composition.

6.1. Minijets

The UA1 minijet studies contain a wealth of information [49-51]. Unfortunately it is difficult to make a precise comparison with the experimental results without a detailed knowledge of the UA1 detector. All results quoted in the following should therefore be understood to refer to a "poor man's" model of the UA1 detector and UA1 minijet reconstruction procedure, as follows [4]. A detector is assumed to stretch between -2.5 and +2.5 in pseudorapidity, evenly divided into 25 layers of cells, with each layer consisting of 24 cells covering the full azimuth. The transverse energy E_T (for massive particles equated with the transverse mass) deposited in each cell is summed. A Gaussian smearing of width $0.5 \cdot E_T^{1/2}$ is imposed cell-by-cell, cut off so that the smeared E_T is never smaller than zero or larger than four times the true value. All bins with $E_T > 1.5$ GeV are taken as possible initiators of jets, and are tried in falling E_T sequence, to check whether the total E_T summed over cells within $\Delta R = \{(\Delta\eta)^2+(\Delta\phi)^2\}^{1/2} \leq 1$ exceeds 5 GeV. If so, these cells together define one jet, with position given by the E_T-weighted center, and are removed from further consideration. Jets which have $|\eta| > 1.5$ or $60^\circ < |\phi| < 120^\circ$ are rejected.

With these constraints, the minijet rate and some simple properties in the nojet and jet samples are shown in Table 2. The number of charged particles and their mean transverse momentum are for particles with $|\eta| < 2.5$; so is the ΣE_T of all particles. The general agreement is good, but there seems to be a tendency in the model to have too large a split in charged multiplicity between the nojet and the jet samples. A part of that discrepancy (but not all) is related to an overestimation in the model of the fraction of events with very low multiplicity in $|\eta| < 2.5$, and may come from an imperfect simulation of UA1 triggering conditions.

6.2. Evidence for Multiple Interactions

The probability that multiple interactions should give rise to two or more pairs of high-p_T jets is small, in particular when compared with the probability to produce high-p_T jets by a single hard interaction with associated initial and final state radiation. It is therefore in the region of relatively small p_T that effects of multiple interactions are expected to influence the multijet rate. This can be studied by comparing the rate of 1-jet, 2-jet, 3-jet and 4-jet events in the UA1 minijet analysis. In fact, most events contain only one jet: although jets should be produced in pairs (neglecting radiation), there are many reasons why only one is observed. Jets are only searched for in some angular regions; a bona fide jet is not found if there is no initiator cell with $E_T > 1.5$ GeV; or a jet may fall below the ΣE_T requirement while its partner does not, by calorimetric fluctuations or fluctuations in the beam jet background.

A steady decrease in rate as the minijet number is increased is therefore to be expected. The decrease in the data [51] is not as marked as in models without multiple interactions, however, see Table 3. Also models with multiple interactions, but without impact parameter dependence or with a simple Gaussian matter distribution, fail to account for the data. A general agreement is obtained with the double Gaussian matter distribution. In principle, the comparison between data and models is marred by uncertainties in the simulation of the UA1 detector. The absolute rate of jet production could also be changed by variations in the K-factor. These two effects would tend to compensate each other, so that the relative pattern should be preserved given e.g. that the 1-jet rate is fixed by data. The case for multiple interactions in the UA1 event sample is therefore strong.

A major uncertainty in the minijet analysis is provided by the calorimetric fluctuations: since the E_T spectrum is rapidly falling, one gains more minijets by upwards fluctuations than one looses by downwards ones. At 630 GeV, the average number of minijets per event would have been 0.112 without fluctuations, but becomes 0.190 with. A helpful cross-check would be to re-do the minijet analysis using only charged particles. One could then reduce the jet initiator minimum E_T to 1 GeV and the minijet E_T threshold to 3 GeV. Assuming that the solid angle covered remains the same, we then obtain almost the same minijet rate as with the "smeared" calorimeter. Also the variation in number of jets and in separation between nojet and jet samples is preserved.

In the future, it would be interesting to study event properties not only for jet and nojet events, but also the evolution of $\langle n_{ch} \rangle$, $\langle p_T \rangle$ etc. as a function of the number of minijets. This should preferentially also be done for smaller jet opening angles, i.e. smaller ΔR.

As noted in the introduction, evidence for multiple interactions has already been presented by the AFS Collaboration [14]. The AFS jets are of about the same ΣE_T but, because of the smaller CM energy (63 GeV), of considerably higher x_T. Therefore the definition of correlated structure functions is more important. Using a simple recipe similar to the one in this paper, the observed rate of double parton scattering is about a factor six higher than expected from Poissonian statistics with no impact parameter dependence [14]. For the double Gaussian matter distribution the average enhancement factor $\langle f(b) \rangle$ in the AFS events should be ≈ 3.7, while a simple Gaussian would give only ≈ 1.7 (the related f_c are 0.92 and 0.89, resepctively, and do not change the picture). The general trend of the UA1 and the AFS data is therefore the same: not only is there evidence for multiple interactions, but at a rate that would suggest regions of denser matter inside the colliding hadrons.

6.3. Correlation Between Multiplicity and Transverse Momentum

The KNO multiplicity distributions for the jet and nojet event samples separately are shown in Fig. 25. One should remember that the seemingly narrow distribution in the jet case is an artefact of using scaled multiplicity; in actual fact the jet event sample at 900 GeV has a width of 17.3 units compared with 8.9 for the nojet one. In our model, KNO scaling does not hold either for the jet or the nojet samples, except as an approximation over some limited energy range.

The average transverse momentum of charged particles (with $|\eta| < 2.5$) has also been studied as a function of the charged multiplicity. Results for 200 GeV are shown in Fig. 26; the corresponding figure for 900 GeV is to be found in [2]. The nojet data are reasonably well reproduced, while agreement is less good for the jet case. At low multiplicities we believe the results to be very sensitive to the details of the minijet trigger, i.e. how often fluctuations in the calorimeter leads to the reconstruction of "false" minijets. The region of high multiplicities is one of the places where the details of the string drawing does matter, as follows. If the flavour assignment of scattered partons and the string drawing between them are chosen so as to minimize the

number of particles produced, then, for a given observed multiplicity, it is necessary to have more interactions (i.e. a smaller p_{T0}). With the summed p_T of scattered partons being large, this is partly inherited by the particles produced. Correspondingly, a maximization of particle production implies the need for fewer interactions and therefore less parton p_T to be shared. The results at 900 GeV are shown in Fig. 27 for the three extreme scenarios implemented in the program: only $q\bar{q}$-scatterings, only gg-scatterings with "maximal" string length, and only gg-scatterings with "minimal" string length. In order to obtain the same average multiplicity in the three cases, the p_{T0} values had to be slightly retuned.

The increase of $\langle p_T \rangle$ with n_{ch} is a high energy phenomenon, and at lower CM energies the opposite behaviour may be observed. This is not unnatural, since multiplicity fluctuations here come less often from a varying number of interactions and more from the fragmentation and decay components. In Fig. 28 one such comparison is presented, with SFM data at 63 and 31 GeV [52]. We do not understand the change in the level of $\langle p_T \rangle$ values between the 31 and 63 GeV data, but the n_{ch} dependence is consistent with model results. On the other hand, the $\langle p_T \rangle$ dependence on n_{ch} will become even more pronounced as the energy is increased, Fig. 29. (Note that the behaviour at small multiplicities is affected by the noninclusion of (double) diffractive events.) The range of populated n_{ch} values is obviously increasing, and so is the $\langle n_{ch} \rangle$, so there is a steady increase with energy of the $\langle p_T \rangle$ of all charged particles, Fig. 30. The trend is enhanced if only central particles, $|\eta| < 2$, are included.

6.4. Jet Profiles

One of the earliest discoveries of jet studies at the $Sp\bar{p}S$ was the "pedestal effect" [35], i.e. that events containing a hard jet also has an above-average particle production away from the jet core. Initial state radiation may account for part of this effect, but not all [29]. Multiple interactions can not solve the problem so long as all collisions are assumed to be equivalent [1], but the introduction of variable impact parameters offers a solution, as follows. Since the average number of jets is larger in central collisions than in peripheral ones, the sample of events containing a hard interaction is biased towards central collisions. These events are then likely to contain additional jet activity. We will now proceed to show that our standard multiple interaction scenario, with a double Gaussian matter distribution, indeed gives a satisfactory agreement with data.

Jet profiles for 5 GeV, 10 GeV and 30 GeV jet triggers are compared with UA1 data at 630 GeV [50] in Fig. 31. The quantity shown is $dE_T/d\eta$ as a function of $\eta-\eta_{jet}$ in the "same side" region $|\phi-\phi_{jet}| < 90^\circ$. One should emphasize that, for the lower jet energies, the profile of the jet core is significantly broadened by the redefinition of the η_{jet} to be the E_T-weighted center rather than the position of the initiator cell.

The average value of the $dE_T/d\eta$ in the range $1 \leqslant |\eta-\eta_{jet}| \leqslant 2$ is shown in Fig. 32 as a function of E_{Tjet}. Note the seeming inconsistency in UA1 data between Fig. 31 and Fig. 32; we choose to trust the latter. The curve has been extended below $E_{Tjet} = 5$ GeV by forming a jet around any initiator cell with $E_T \geqslant 1.5$ GeV. The rise of $\langle dE_T/d\eta \rangle$ up to $E_{Tjet} \approx 12$ GeV is due to a shift in the composition of events, from one dominated by fairly peripheral collisions to one strongly biased towards central ones. In the model, there is a limit for how far this biasing can go: once

$$\int_{p_T}^{s^{1/2}/2} \frac{d\sigma}{dp_T'}\, dp_T' = \sigma_{hard}(p_T) \ll \sigma_{nd} \tag{39}$$

the exponential in eq. (34) can be neglected. The probability distribution in b is then given by $\tilde{O}(b)\, d^2b$, independently of the p_T value. The condition (39) is fulfilled for $p_T \approx E_{Tjet} \approx 10$ GeV, leading to a plateau above that. There is even a slight drop with energy, due to a change from predominantly gluon-gluon scatterings to predominantly quark-quark ones [29]. By comparison, in a scenario without multiple interactions, there is no natural mechanism for obtaining a significant pedestal effect, Fig. 32. Furthermore, whereas the E_{Tjet} value where a plateau is attained is a stable prediction of the model, the height of that plateau is sensitive to the hadronic matter distribution assumed. The standard double Gaussian here gives a good description.

At higher energies, the level of the plateau is predicted to increase successively, but the E_{Tjet} value where the plateau starts will vary only slowly. In Fig. 33 some jet profiles at 2, 10 and 40 TeV (still using the UA1 inspired jet algorithm; results could well be slightly different with the actual CDF/D0 etc. reconstruction procedures) are shown. Fig. 34 contains the predictions for the plateau level $\langle dE_T/d\eta \rangle(E_{Tjet})$ in $1 \leqslant |\eta-\eta_{jet}| \leqslant 2$.

7. Summary and Outlook

In this paper we have tried to present a realistic model for particle production in hadron-hadron collisions. If the measure of success is the degree of simplicity achieved, then ours is a complete failure. From physics considerations, backed by comparisons with data, we have been led to the formulation of a very complex and detailed model. The list of factors that influence the multiplicity distribution (section 5.2) contains six major points, each of which requires the development of specific models, and each of which has a number of free parameters. And yet, it is very difficult to imagine how any of the six points could be discarded in order to obtain a simpler model. It is therefore likely that a better model would also have to be an even more detailed one.

Considering the complexity and the number of unanswered questions, is it meaningful to trust the model at all? Probably yes, at least up to a point. Many of the components can be independently checked: fragmentation and parton showers in e^+e^- annihilation, hard parton-parton interactions (whether one per event or more) by jet studies, and so on. In this paper we have presented several successful comparisons with data, and a few not so successful. In particular, the model provides an understanding of the event rate of multiple minijet production and the variation of pedestal level with jet energy, effects which are not easily accommodated in simpler models. The main problem seems to be the understanding of low-multiplicity events, be that double diffractive or whatever. Since the complete model is publicly available in Monte Carlo form [3,4], further checks could be made in the context of more realistic detector simulations.

In addition, different uncertainties do not necessarily add up the way one might expect. If some detail in the model is varied, generally the p_{T0} scale has to be retuned somewhat to retain the same average charged multiplicity, and the two changes usually tend to compensate each other. This is one of the reasons why the major uncertainties in string drawing issues (and in quark/gluon composition of scattered flavours) are not all that important for the overall picture.

It is easy to enumerate aspects where further studies ought to be made, if only one knew how. The model contains none of the quantum mechanical complexities that must be there, such as interference effects between different semihard interactions. The simultaneous definition of structure

functions for several partons inside a hadron is achieved in the most naive fashion possible. The whole description of a hadronic matter distribution for the colliding hadrons, with the spatial distribution of partons completely decoupled from the momentum distribution, is overly simplistic. The regularization of the perturbative QCD cross-section at small p_T values, although not unreasonable, is certainly arbitrary. A description in terms of independently fragmenting simple colour strings may or may not be a good approximation to what is actually happening. The choice of colour flow structure is only a first attempt. Multiple interactions could come from one initial parton cascading into many, whereof several scatter against partons in the colliding hadron; this could actually be the reason why we were forced to introduce local concentrations of matter inside the hadrons.

In conclusion, the model presented here offers a description of high-p_T and low-p_T phenomena within one single framework. It may be used as a base on which further developments could be added. The ultimate objective, to provide a description of all particle production phenomena in hadron collisions, is obviously not yet within reach. Important further tests of the basic ideas will already come with the data from the new Tevatron I Collider and, on a longer time scale, with the advent of SSC/LHC.

Acknowledgements

We would like to thank H.-H. Thodberg for stimulating discussions on the AFS jet studies and H.-U. Bengtsson for inspiring collaboration in the development of PYTHIA. One of us (T.S.) would also like to thank C. Wulz for helpful discussions on the UA1 minijet analysis.

References

1. T. Sjöstrand, FERMILAB-Pub-85/119-T (1985)

2. T. Sjöstrand, M. van Zijl, LU TP 86-25, to appear in Phys. Lett. B

3. H.-U. Bengtsson, T. Sjöstrand, LU TP 87-3/UCLA-87-001, submitted to Computer Phys. Comm.

4. T. Sjöstrand, Computer Phys. Comm. 39 (1986) 347
   T. Sjöstrand, M. Bengtsson, Computer Phys. Comm. 43 (1987) 367

5. P. V. Landshoff, J. C. Polkinghorne, Phys. Rev. D18 (1978) 3344
   C. Goebel, D. M. Scott, F. Halzen, Phys. Rev. D22 (1980) 2789

6. N. Paver, D. Treleani, Nuovo Cimento 70A (1982) 215, ibid. 73A (1983) 392, Phys. Lett. 146B (1984) 252, Z. Physik C28 (1985) 187

7. B. Humpert, Phys. Lett. 131B (1983) 461
   B. Humpert, R. Odorico, Phys. Lett. 154B (1985) 211

8. V. A. Abramovski. O. V. Kancheli, V. N. Gribov, in Proc. of the XVI International Conference on High Energy Physics, eds. J. D. Jackson, A. Roberts, R. Donaldson, vol 1, p. 389

9. A. Capella, J. Tran Thanh Van, Phys. Lett. 114B (1982) 450, Z. Physik C18 (1983) 85, Z. Physik C23 (1984) 165
   A. Capella, A. Staar, J. Tran Thanh Van, Phys. Rev. D32 (1985) 2933

10. P. Aurenche, F. W. Bopp, Phys. Lett. 114B (1982) 363
    P. Aurenche, F. W. Bopp, J. Ranft, Z. Physik C23 (1984) 67, Z. Physik C26 (1984) 279, Phys. Lett. 147B (1984) 212

11. K. Fiałkowski, A. Kotanski, Phys. Lett. 107B (1981) 132, ibid. 115B (1982) 425
    A. B. Kaidalov, Phys. Lett. 116B (1982) 459

    A. B. Kaidalov, K. A. Ter Martirosyan, Phys. Lett. 117B (1982) 247

12. A. Białas, E. Białas, Acta. Phys. Pol. B5 (1974) 373 and references therein
    T. T. Chou, C. N. Yang, Phys. Rev. D32 (1985) 1692
    S. Barshay, Z. Physik C32 (1986) 513
    W. R. Chen, R. C. Hwa, University of Oregon preprint OITS-347 (1986)

13. T. T. Chou, C. N. Yang, Phys. Rev. 170 (1968) 1591, Phys. Rev. D19 (1979) 3268
    C. Bourrely, J. Soffer, T. T. Wu, Nucl. Phys. B247 (1984) 15
    P. L'Heureux, B. Margolis, P. Valin, Phys. Rev. D32 (1985) 1681
    L. Durand, H. Pi, Phys. Rev. Lett. 58 (1987) 303

14. AFS Collaboration, T. Åkesson et al., CERN-EP/86-216 (1986)

15. E. Eichten, I. Hinchliffe, K. Lane, C. Quigg, Rev. Mod. Phys. 56 (1984) 579, ibid. 58 (1986) 1065

16. R. K. Ellis, J. C. Sexton, Nucl. Phys. B269 (1986) 445

17. L. V. Gribov, E. M. Levin, M. G. Ryskin, Phys. Rep. 100 (1983) 1

18. A. H. Mueller, J. Qiu, Nucl. Phys. B268 (1986) 427

19. J. P. Ralston, D. W. McKay, FERMILAB-Pub-86/95-T (1986)

20. J. C. Collins, in Observable Standard Model Physics at the SSC: Monte Carlo Simulation and Detector Capabilities, eds. H.-U. Bengtsson, C. Buchanan, T. Gottschalk, A. Soni (World Scientific, Singapore, 1986), p. 15

21. M. M. Block, R. N. Cahn, Rev. Mod. Phys. 57 (1985) 563
    M. M. Block, talk presented at XXIst Rencontre de Moriond, France, March 16-22, 1986

22. K. Goulianos, Phys. Rep. 101 (1983) 169

23. J. Kuti, V. F. Weisskopf, Phys. Rev. D4 (1971) 3418
    H. R. Gerhold, Nuovo Cimento 59A (1980) 373

24. A. Capella, J. Tran Thanh Van, Z. Physik C10 (1981) 249

25. A. Capella, U. Sukhatme, C. I. Tan, J. Tran Thanh Van, Phys. Lett. 81B (1979) 68

26. G. Gustafson, Z. Physik C15 (1982) 155
H.-U. Bengtsson, Computer Phys. Comm. 31 (1984) 323

27. M. Bengtsson, T. Sjöstrand, LU TP 86-18, to appear in Phys. Lett. B, LU TP 86-24, to appear in Nucl. Phys. B

28. A. H. Mueller, Phys. Lett. 104B (1981) 161
B. I. Ermolaev, V. S. Fadin, JETP Lett. 33 (1981) 269
A. Bassetto, M. Ciafaloni, G. Marchesini, Phys. Rep. 100 (1983) 201
G. Marchesini, B. R. Webber, Nucl. Phys. B238 (1984) 1

29. T. Sjöstrand, Phys. Lett. 157B (1985) 321
M. Bengtsson, T. Sjöstrand, M. van Zijl, Z. Physik C32 (1986) 67

30. B. Andersson, G. Gustafson, G. Ingelman, T. Sjöstrand, Phys. Rep. 97 (1983) 33

31. T. Sjöstrand, Phys. Lett. 142B (1984) 420, Nucl. Phys. B248 (1984) 469

32. UA5 Collaboration, G. J. Alner et al., Phys. Lett. 138B (1984) 304

33. J. Gaudaen, Ph. D. Thesis, Universiteit Antwerpen (1984)

34. J. G. Rushbrooke, in Proc. of $p\bar{p}$ Options for the Supercollider, eds. J. A. Pilcher, A. R. White, p. 176

35. UA1 Collaboration, G. Arnison et al., Phys. Lett. 132B (1983) 214

36. G. E. Brown, M. Rho, Phys. Lett. 82B (1979) 177

37. I. Montvay, Phys. Lett. 84B (1979) 331

38. S. Fredriksson, M. Jändel, T. Larsson, Z. Physik C19 (1983) 53

39. A. Breakstone et al., Z. Physik C28 (1985) 335

40. G. Ingelman, P. E. Schlein, Phys. Lett. 152B (1985) 256

41. UA5 Collaboration, G. J. Alner et al., Phys. Lett. 167B (1986) 476

42. Z. Koba, H. B. Nielsen, P. Olesen, Nucl. Phys. B40 (1972) 317

43. T. V. Gaisser, F. Halzen, Phys. Rev. Lett. 54 (1985) 1754
G. Pancheri, Y. Srivastava, Phys. Lett. 159B (1985) 69
A. D. Martin, C. J. Maxwell, Phys. Lett. 172B (1986) 248

44. P. Carruthers, C. C. Shih, Phys. Lett. 127B (1983) 242
C. S. Lam, M. A. Walton, Phys. Lett. 140B (1984) 246
A. Giovanni, L. Van Hove, Z. Physik C30 (1986) 391
B. Durand, I. Sarcevic, Phys. Lett. 172B (1986) 104

45. UA5 Collaboration, G. J. Alner et al., Z. Physik C33 (1986) 1

46. UA5 Collaboration, G. J. Alner et al., CERN-EP/86-213

47. UA5 Collaboration, G. J. Alner et al., Phys. Lett. 160B (1985) 193

48. UA5 Collaboration, G. J. Alner et al., Nucl. Phys. B258 (1985) 505

49. F. Ceradini (UA1 Collaboration), in Proc. of International Europhysics Conference on High Energy Physics, eds. L. Nitti, G. Preparata (Laterza, Bari, 1985), p. 363

50. C. Albajar (UA1 Collaboration), to appear in Proc. of the Workshop on Physics Simulation at High Energy, Madison, Wisconsin, USA, May 5 - 16, 1986
A. Di Ciaccio (UA1 Collaboration), to appear in Proc. of XVII International Symposium on Multiparticle Dynamics, Seewinkel, Austria, June 16 - 20, 1986
F. Lacava (UA1 Collaboration), to appear in Proc. of the 6th Topical Workshop on Proton-Antiproton Physics, Aachen, Germany, June 30 - July 4, 1986

51. C. Wulz (UA1 Collaboration), talk presented at XXIInd Rencontre de Moriond, France, March 15 - 21, 1987

52. A. Breakstone et al., Phys. Lett. 132B (1983) 463

Table 1

Moments of the multiplicity distribution at 200, 540 and 900 GeV, UA5 data [41] compared with model results.

	200 GeV		540 GeV		900 GeV	
	UA5	model	UA5	model	UA5	model
$\langle n \rangle$	21.4±0.8	21.0	29.1±0.9	28.8	34.6±1.2	34.7
D	10.9±0.4	9.9	16.3±0.4	15.8	20.2±0.6	20.5
$\langle n \rangle / D$	1.96±0.09	2.11	1.79±0.06	1.82	1.72±0.07	1.69
C_2	1.26±0.03	1.22	1.31±0.03	1.30	1.34±0.03	1.35
C_3	1.91±0.12	1.80	2.12±0.11	2.18	2.22±0.13	2.40
C_4	3.3±0.3	3.2	4.1±0.3	4.6	4.3±0.4	5.4

Table 2

Minijet phenomenology, comparison between UA1 data [49] and model results. Quoted UA1 errors are statistical only. $\langle n_{ch} \rangle$ and $\langle p_T \rangle$ are evaluated for the region $|\eta| < 2.5$.

	200 GeV		900 GeV	
	UA1	model	UA1	model
jet event fraction (%)	5.9	5.7	17.2	15.0
$\langle n_{ch} \rangle_{nojet}$	13.81±0.07	11.9	15.93±0.07	14.4
$\langle n_{ch} \rangle_{jet}$	26.49±0.23	27.9	32.89±0.13	34.2
$\langle p_T \rangle_{nojet}$ (GeV)	0.382±0.005	0.385	0.411±0.005	0.400
$\langle p_T \rangle_{jet}$ (GeV)	0.474±0.007	0.453	0.516±0.006	0.496

Table 3

Jet rate and other properties of jet and nojet events at 630 GeV, UA1 data [51,49] and different models. $\langle n_{ch}\rangle$, $\langle p_T\rangle$ and $\langle \Sigma E_T\rangle$ are evaluated for the region $|\eta| < 2.5$.

	UA1	no multiple interactions	impact parameter independent	simple Gaussian	double Gaussian
≥1 jet fraction (%)	14.8	17.0	14.3	13.7	12.6
1 jet fraction (%)	9.96	14.30	11.51	10.79	8.88
2 jet fraction (%)	3.45	2.45	2.45	2.70	2.67
3 jet fraction (%)	1.12	0.22	0.32	0.19	0.74
4 jet fraction (%)	0.22	0.01	0.04	0.05	0.25
5 jet fraction (%)	0.05	0.00	0.00	0.01	0.07
$\langle n_{ch}\rangle_{nojet}$	15.06	14.3	11.9	13.5	12.9
$\langle n_{ch}\rangle_{jet}$	32.21	23.7	26.6	30.9	34.2
$\langle p_T\rangle_{nojet}$ (GeV)	0.407	0.415	0.398	0.395	0.392
$\langle p_T\rangle_{jet}$ (GeV)	0.502	0.508	0.515	0.473	0.471
$\langle \Sigma E_T\rangle_{nojet}$ (GeV)		13.5	11.0	12.4	12.5
$\langle \Sigma E_T\rangle_{jet}$ (GeV)		26.2	29.3	32.1	38.2

Figure Captions

Fig. 1. The integrated parton-parton cross-section $\sigma_{hard}(p_{Tmin})$ as a function of the p_{Tmin} cutoff scale. Curves are, from bottom to top, for 63 GeV, 540 GeV, 5 TeV and 40 TeV, respectively. No effective K-factors are included here.

Fig. 2. Schematic view of colour string drawing in hadron collisions. Full lines indicate strings, dashed outline outgoing hadron remnants, with a dot for each valence quark (antiquark) and an extra ellipse marking an effective diquark (antidiquark).
a) Baryon-baryon collision.
b) Baryon-antibaryon collision.
c) Baryon-antibaryon collision containing a hard gluon-gluon scattering.

Fig. 3. Charged multiplicity distribution at 540 GeV, UA5 results [32] vs. simple models: dashed low-p_T only, full including hard scatterings, dash-dotted also including initial and final state radiation.

Fig. 4. Forward-backward multiplicity correlation at 540 GeV, UA5 results [33] vs. simple models; latter with notation as in Fig. 3.

Fig. 5. Charged multiplicity distribution at 540 GeV, UA5 results [32] vs. impact parameter independent multiple interaction model: dashed p_{Tmin} = 2.0 GeV, full p_{Tmin} = 1.6 GeV, dash-dotted p_{Tmin} = 1.2 GeV.

Fig. 6. Forward-backward multiplicity correlation at 540 GeV, UA5 results [33] vs. impact parameter independent multiple interaction model; latter with notation as in Fig. 5.

Fig. 7. Jet energy profile for E_{Tjet} > 35 GeV at 540 GeV, UA1 data [35] vs. model results: dashed without multiple interactions, full with multiple interactions (impact parameter independent), dash-dotted with multiple interaction rate arbitrarily increased by a factor four.

Fig. 8. Values for the cutoff parameter p_{T0} as a function of CM energy, as determined from comparisons with the average charged multiplicity. Dashed with a logarithmic extrapolation to higher energies, eq. (38), dotted if assumed constant above 900 GeV.

Fig. 9. The average number of interactions per nondiffractive event as a function of CM energy. Extrapolations shown correspond to the two extremes of Fig. 8.

Fig. 10. Variation of the total inelastic, nondiffractive cross-section obtained in the variable impact parameter picture, normalized to a standard parametrization [21,22] at 540 GeV. Dashed model results (with p_{T0} = 2 GeV above 900 GeV), full the parametrization.

Fig. 11. Schematic view of the three string drawing possibilities that are used, evenly mixed, to describe subsequent interactions. For notation cf. Fig. 2.; in addition thick lines denote scattered quarks.
a) Double string between scattered gluons.
b) Simple string between scattered $q\bar{q}$ pair.
c) Scattered gluons attached to nearby string pieces.

Fig. 12. Charged multiplicity distribution at 540 GeV, UA5 results [32] vs. multiple interaction model with variable impact parameter: full double Gaussian matter distribution, dashed with fix impact parameter (i.e. $\delta_0(b)$).

Fig. 13. Separation of multiplicity distribution at 540 GeV by number of interactions in event for double Gaussian matter distribution. Long dashes (double) diffractive, dash-dotted one interaction, thick full two, dashed three, dotted four or more, thin full sum of everything.

Fig. 14. Average charged multiplicity as a function of the number of interactions. Full line at 540 GeV, dashed at 5 TeV, dash-dotted at 40 TeV.

Fig. 15. Average charged multiplicity as a function of the "enhancement factor" $f(b)$. Notation as in Fig. 14.

Fig. 16. Average charged multiplicity for nondiffractive events as a function of CM energy. Dotted assuming p_{T0} = 2.0 constant above 540 GeV, dashed using the logarithmic extrapolation of eq. (38), cf. Fig. 8.

Fig. 17. Predicted multiplicity distributions for higher energies, taking p_{T0} = 2.0 GeV and assuming a double Gaussian matter distribution. Dash-dotted at 1.6 TeV, dashed at 5 TeV, dotted at 15 TeV and full at 40 TeV.

Fig. 18. Scaled multiplicity distribution (KNO plot [42]) at 40 TeV. Dashed with fix impact parameter (δ_0), dotted with Gaussian and full with double Gaussian matter distribution.

Fig. 19. Ratio $D/\langle n\rangle$, i.e. the dispersion over the mean value for the charged multiplicity distribution, as a function of the CM energy, shown as different pieces of physics are successively added on. Lower dashed a one-string scenario, lower full simple two-string model, dash-dotted including a hard interaction with initial and final state radiation, dotted with multiple interactions in the impact parameter independent scenario, upper dashed with variable impact parameters and upper full including double diffractive events.

Fig. 20. Charged particle pseudorapidity distribution at 200 GeV, 540 GeV and 900 GeV, from bottom to top. Data points from UA5 [45].

Fig. 21. Charged particle pseudorapidity distribution at 540 GeV for different bins in total charged multiplicity. From bottom to top for $n_{ch} \leq 10$, 12 - 20, 42 - 50 and 72 - 80. Data points from UA5 [46].

Fig. 22. Scaled multiplicity distributions in pseudorapidity bins, model compared with UA5 data at 540 GeV [47].

Fig. 23. Forward-backward multiplicity correlations at 540 GeV, UA5 results [33] vs. multiple interaction model: full double Gaussian matter distribution, dashed with fix impact parameter (δ_0).

Fig. 24. The K/π ratio as a function of transverse momentum, UA5 data points [48] and model results.

Fig. 25. Scaled multiplicity plots for a) minijet events, b) nojet events. Full line shows average UA1 data in the range 200 - 900 GeV [49],

dashed model results at 200 GeV, dotted at 900 GeV.

Fig. 26. Average transverse momentum of charged particles in $|\eta| < 2.5$ as a function of the multiplicity, for jet and nojet samples separately. UA1 data points at 200 GeV [49] compared with model results.

Fig. 27. Average transverse momentum of charged particles in $|\eta| < 2.5$ as a function of the multiplicity. UA1 data points [49] at 900 GeV compared with the model for different assumptions about the nature of the subsequent (non-hardest) interactions. Dashed assuming $q\bar{q}$-scatterings only, dotted gg-scatterings with "maximal" string length, full gg-scatterings with "minimal" string length.

Fig. 28. Average transverse momentum of charged particles in $|\eta| < 2$ as a function of the multiplicity, SFM data points at 63 and 31 GeV [52] vs. model curves, full at 63 GeV and dashed at 31 GeV.

Fig. 29. Average transverse momentum of charged particles in $|\eta| < 2.5$ as a function of the multiplicity, full curve at 540 GeV, dotted at 5 TeV and dashed at 40 TeV. Only nondiffractive events are included.

Fig. 30. Average transverse momentum as a function of the CM energy, full for all charged particles, dashed for charged particles with $|\eta| < 2$.

Fig. 31. Jet profiles, $dE_T/d\eta$ as a function of $\eta-\eta_{jet}$, in the "same side" region $|\phi-\phi_{jet}| < 90^o$. Histograms are UA1 data at 630 GeV [50], curves model results.

a) $E_{Tjet} > 5$ GeV.

b) $E_{Tjet} > 10$ GeV.

c) $E_{Tjet} > 30$ GeV.

Fig. 32. Average transverse energy $\langle dE_T/d\eta\rangle$ in $1 \leqslant |\eta-\eta_{jet}| \leqslant 2$, $|\phi-\phi_{jet}| < 90^o$ as a function of the E_{Tjet} trigger. Data points UA1 at 630 GeV [50], dashed curve with impact parameter independent model, dotted with Gaussian and full with double Gaussian matter distribution.

Fig. 33 Jet profiles, $dE_T/d\eta$ as a function of $\eta-\eta_{jet}$, in the "same side" region $|\phi-\phi_{jet}| < 90^o$. Full model results at 2 TeV, dashed at 10 TeV and dotted at 40 TeV (with UA1 inspired jet algorithm).

a) $E_{Tjet} > 5$ GeV.

b) $E_{Tjet} > 10$ GeV.

c) $E_{Tjet} > 30$ GeV.

Fig. 34. Average transverse energy $\langle dE_T/d\eta\rangle$ in $1 \leqslant |\eta-\eta_{jet}| \leqslant 2$, $|\phi-\phi_{jet}| < 90^o$ as a function of the E_{Tjet} trigger (UA1 inspired jet algorithm). Full curve at 2 TeV, dashed at 10 TeV and dotted at 40 TeV.

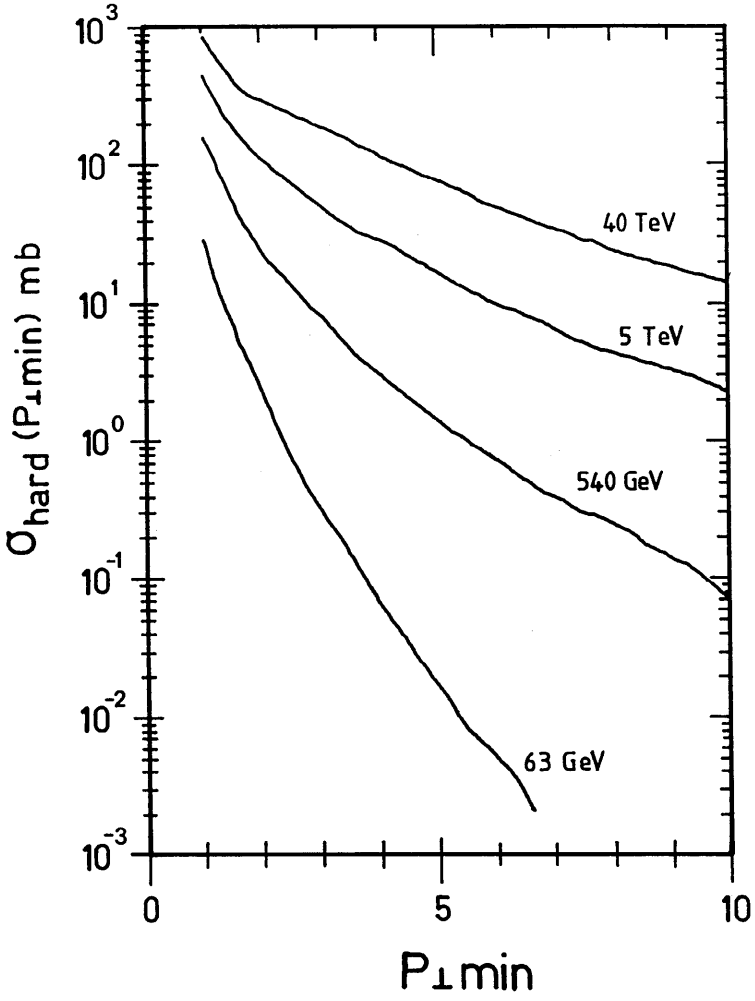
10^3
10^2
10^1
10^0
10^{-1}
10^{-2}
10^{-3}
σ_{hard} ($P_\perp$min) mb
40 TeV
5 TeV
540 GeV
63 GeV
0
5
10
$P_\perp$min

FIG. 1

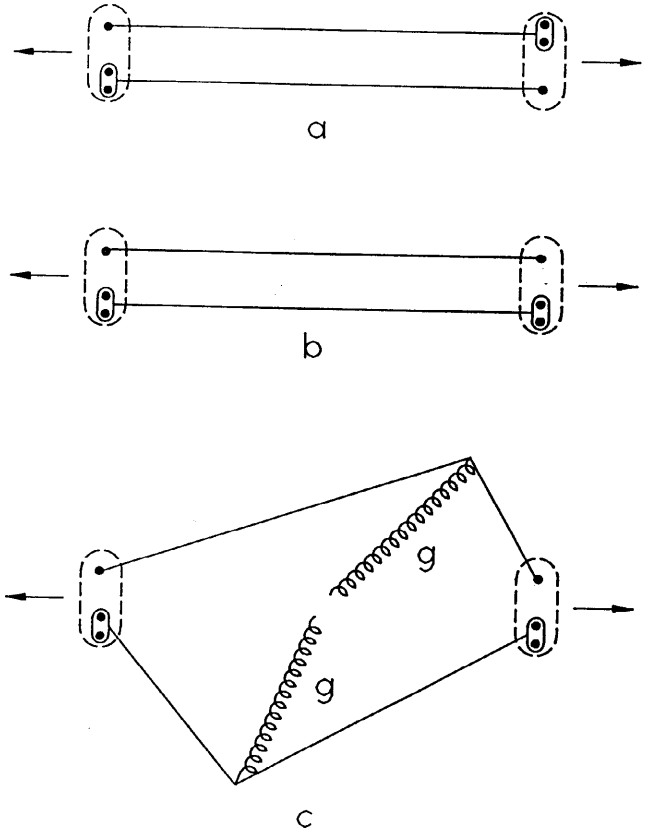
a
b
g
g
c

FIG. 2

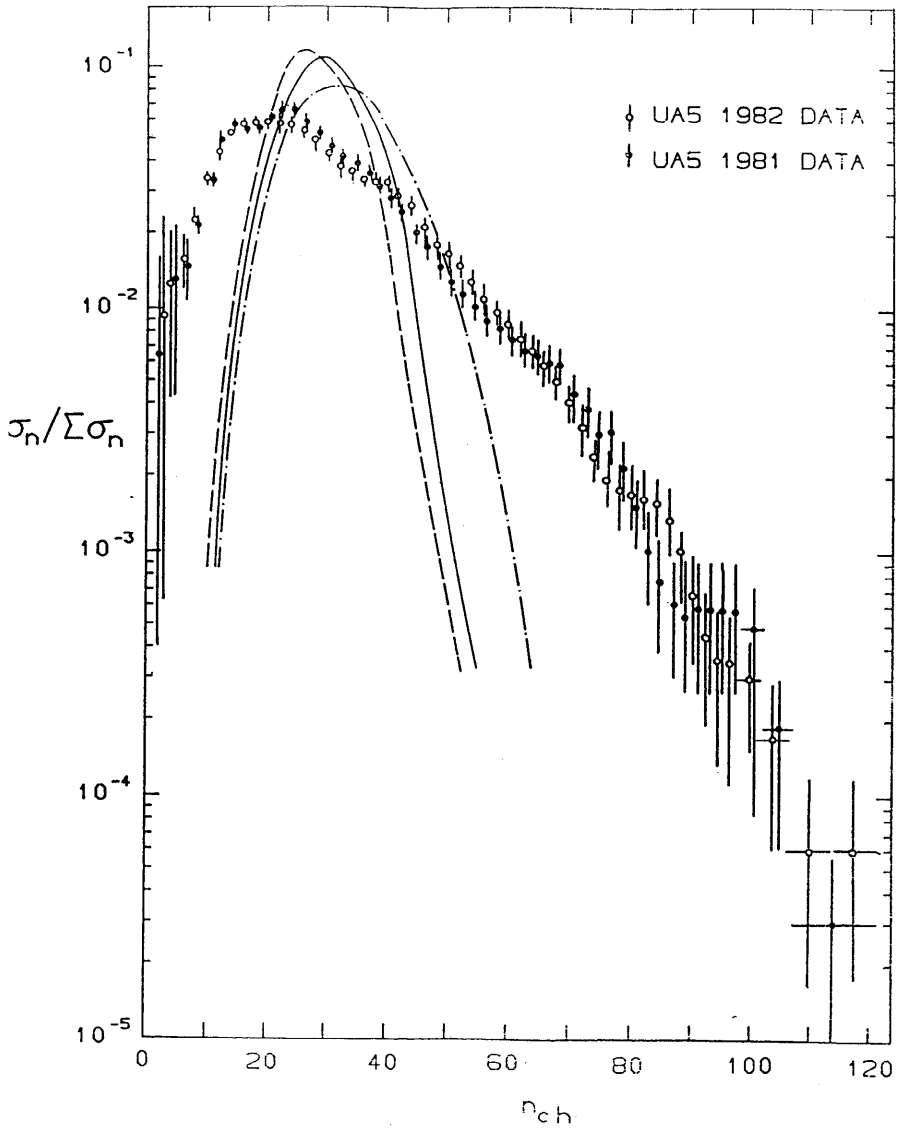
UA5 1982 DATA
UA5 1981 DATA
$\sigma_n/\Sigma\sigma_n$
n_{ch}

FIG. 3

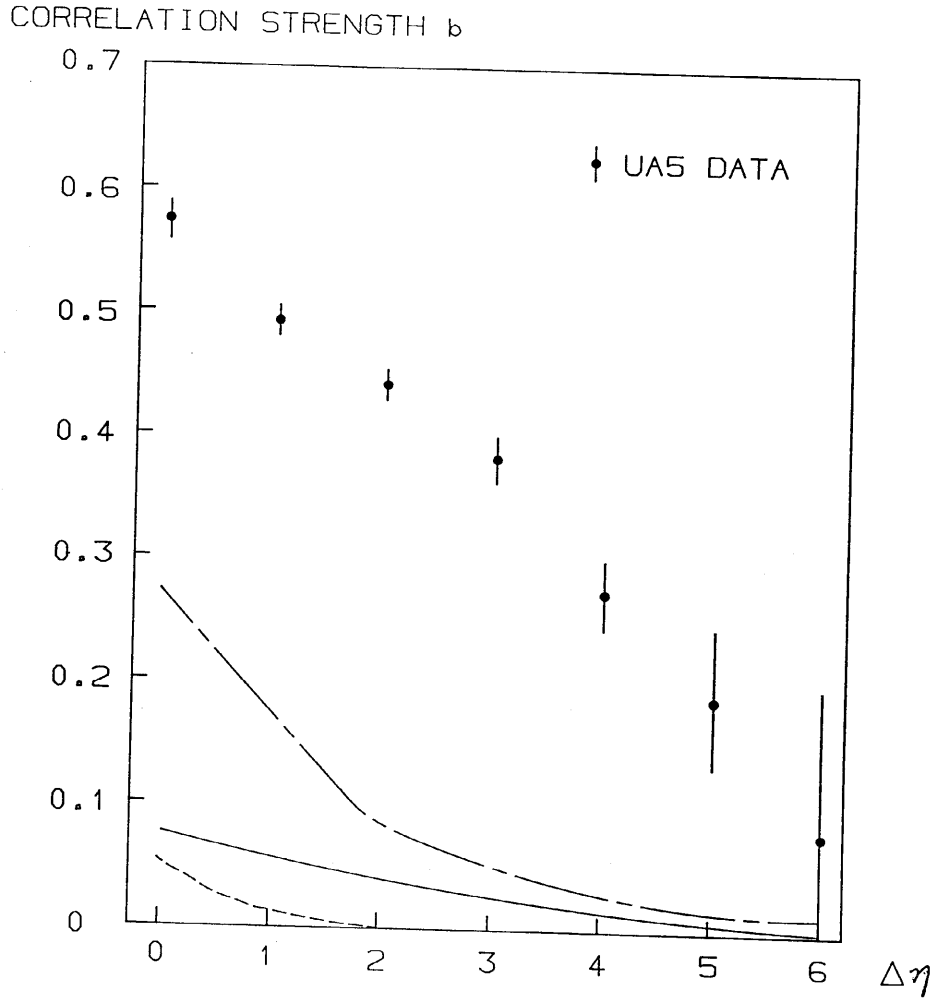
CORRELATION STRENGTH b
UA5 DATA
$\Delta\eta$

FIG. 4

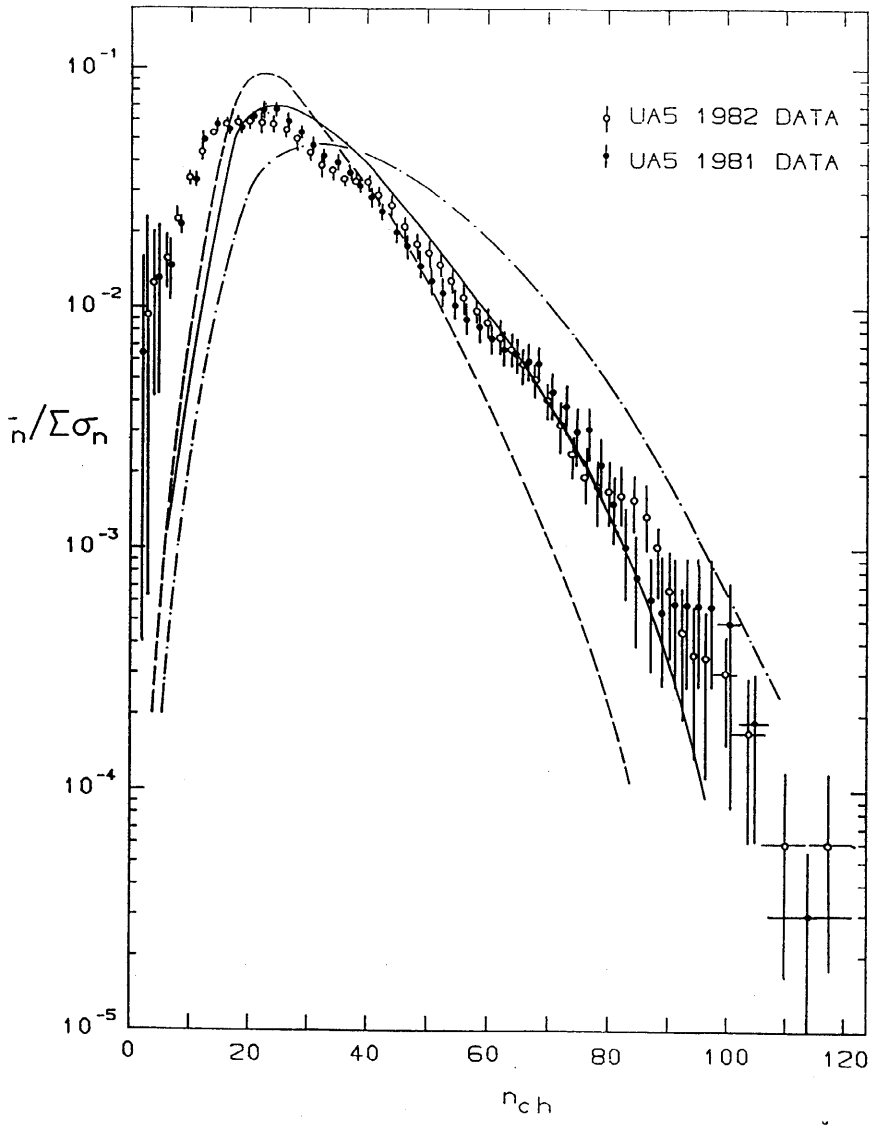
UA5 1982 DATA
UA5 1981 DATA
$\bar{n}/\Sigma\sigma_n$
n_{ch}

FIG. 5

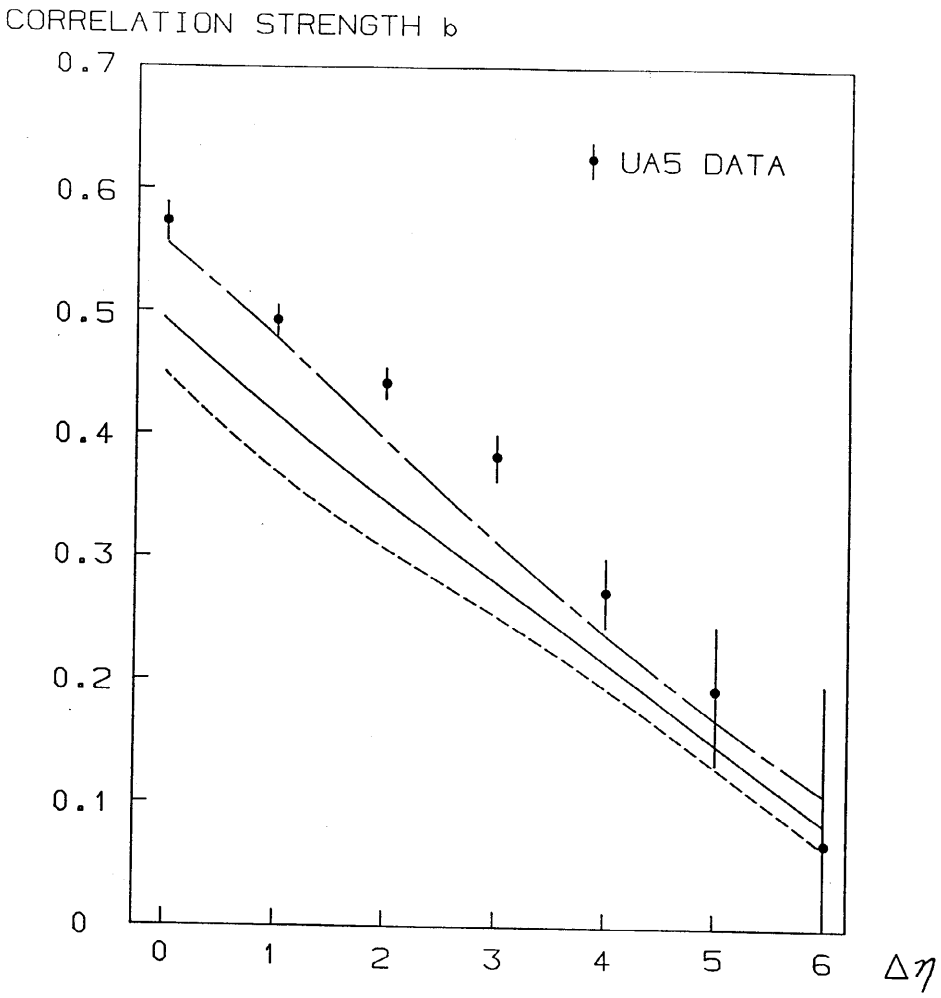
CORRELATION STRENGTH b
UA5 DATA
$\Delta\eta$

FIG. 6

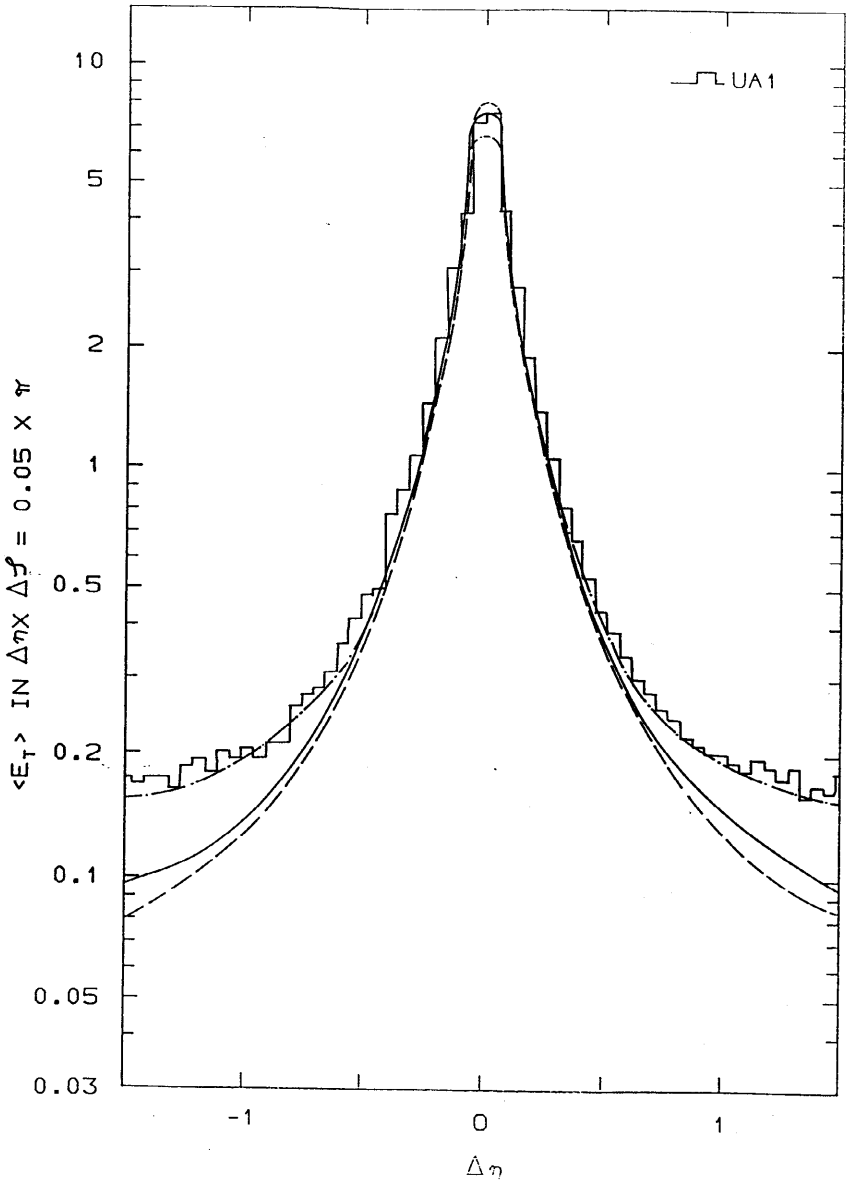
UA1
10
5
2
1
0.5
0.2
0.1
0.05
0.03
-1
0
1
$\Delta\eta$
$\langle E_T \rangle$ IN $\Delta\eta \times \Delta\varphi = 0.05 \times \pi$

FIG. 7

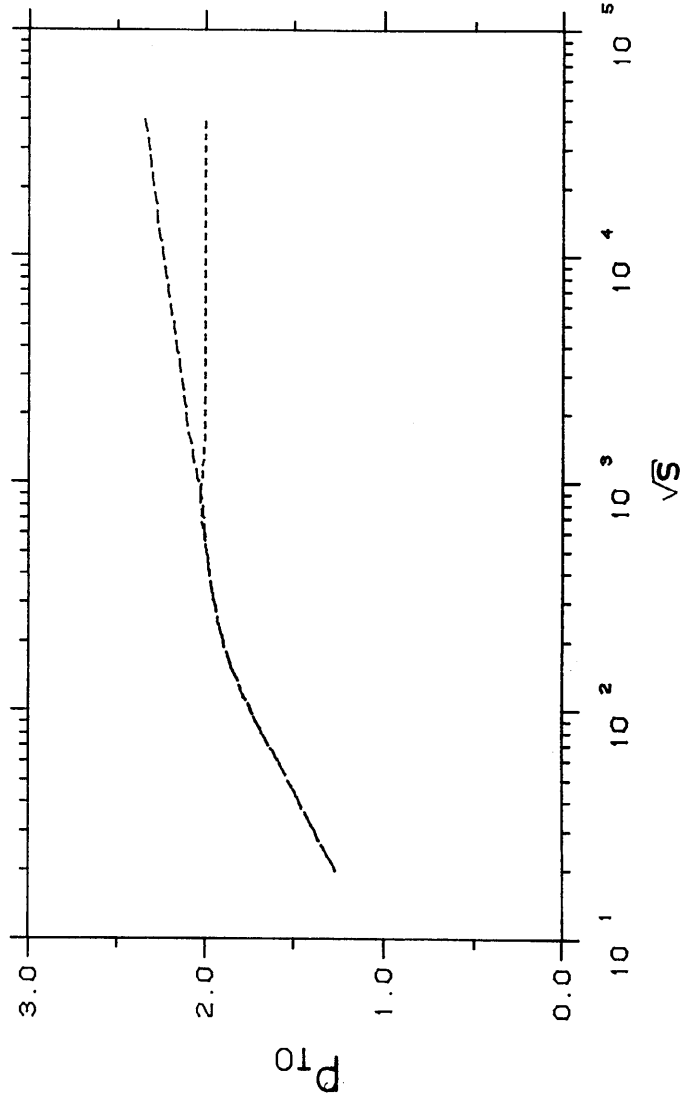
p_{T0}
3.0
2.0
1.0
0.0
10^1
10^2
10^3
10^4
10^5
$\sqrt{s}$

FIG. 8

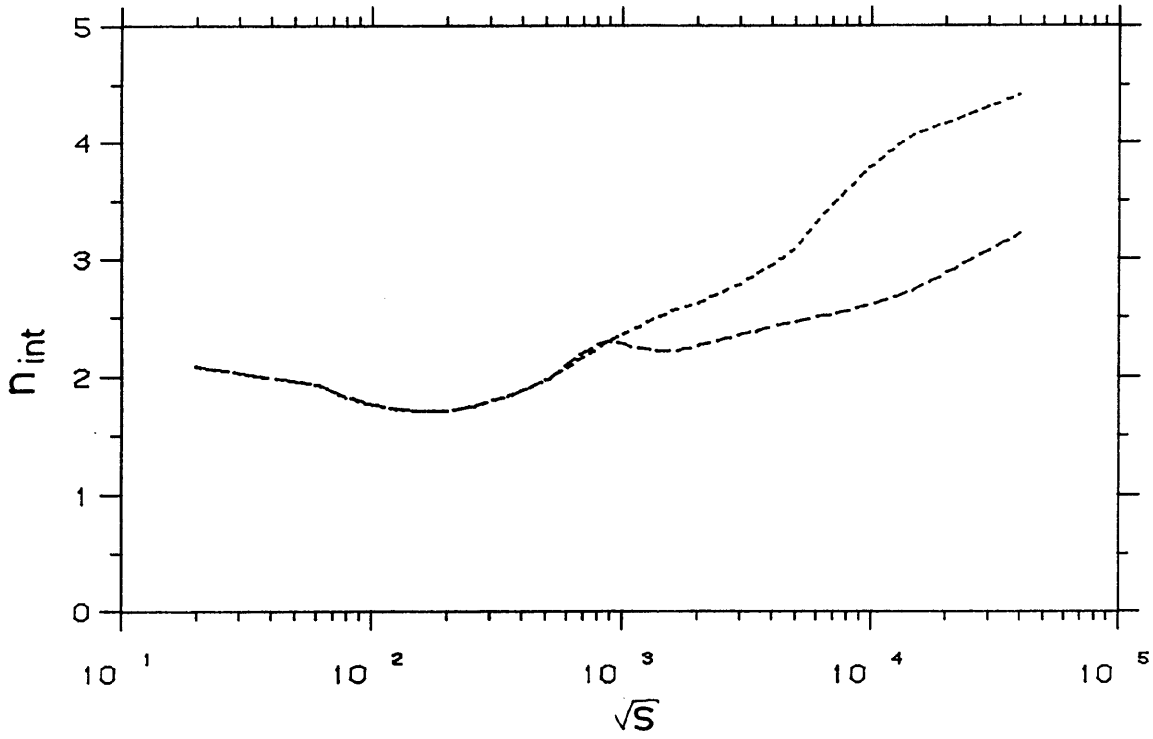
n_{int}
0
1
2
3
4
5
10^1
10^2
10^3
10^4
10^5
$\sqrt{s}$

FIG. 9

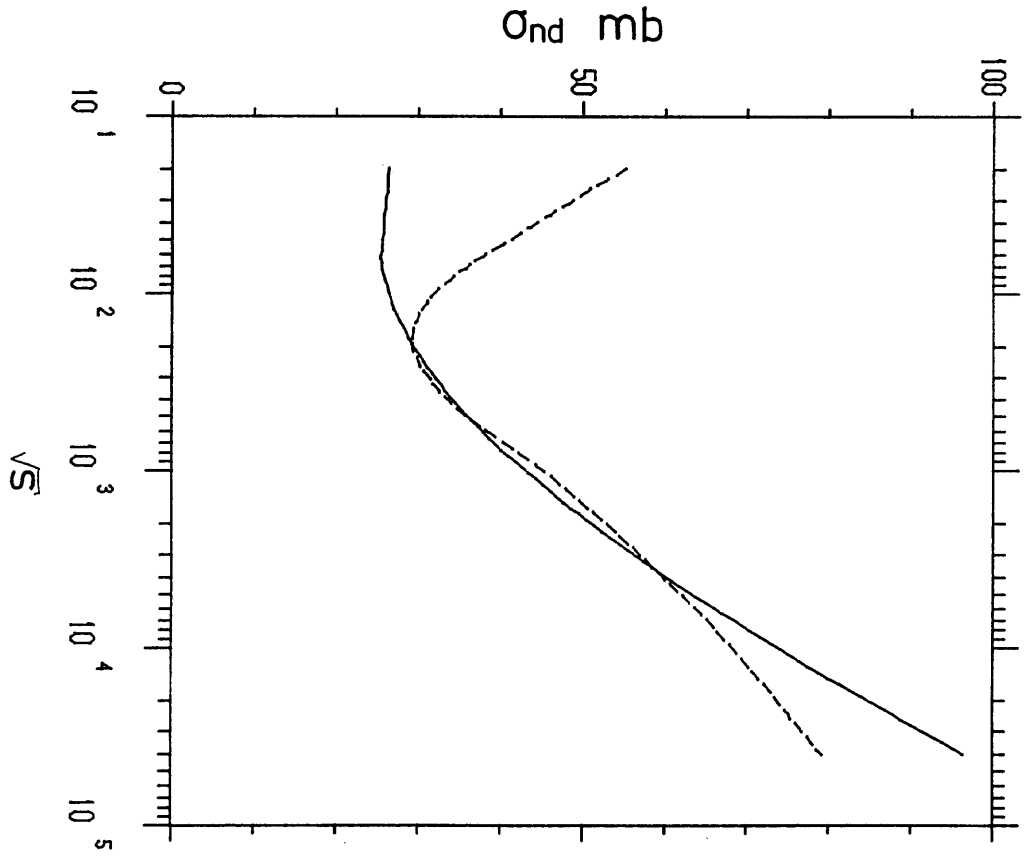
σ_{nd} mb
0
50
100
10^1
10^2
10^3
10^4
10^5
$\sqrt{s}$

FIG. 10

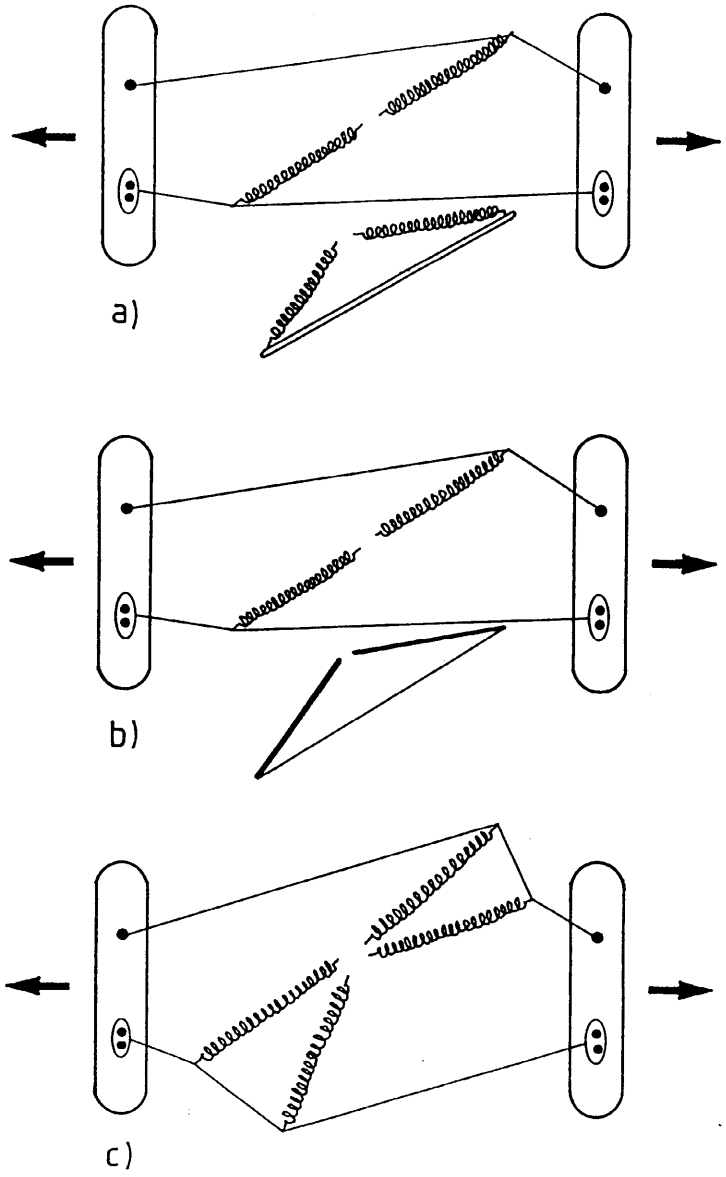
a)
b)
c)

FIG. 11

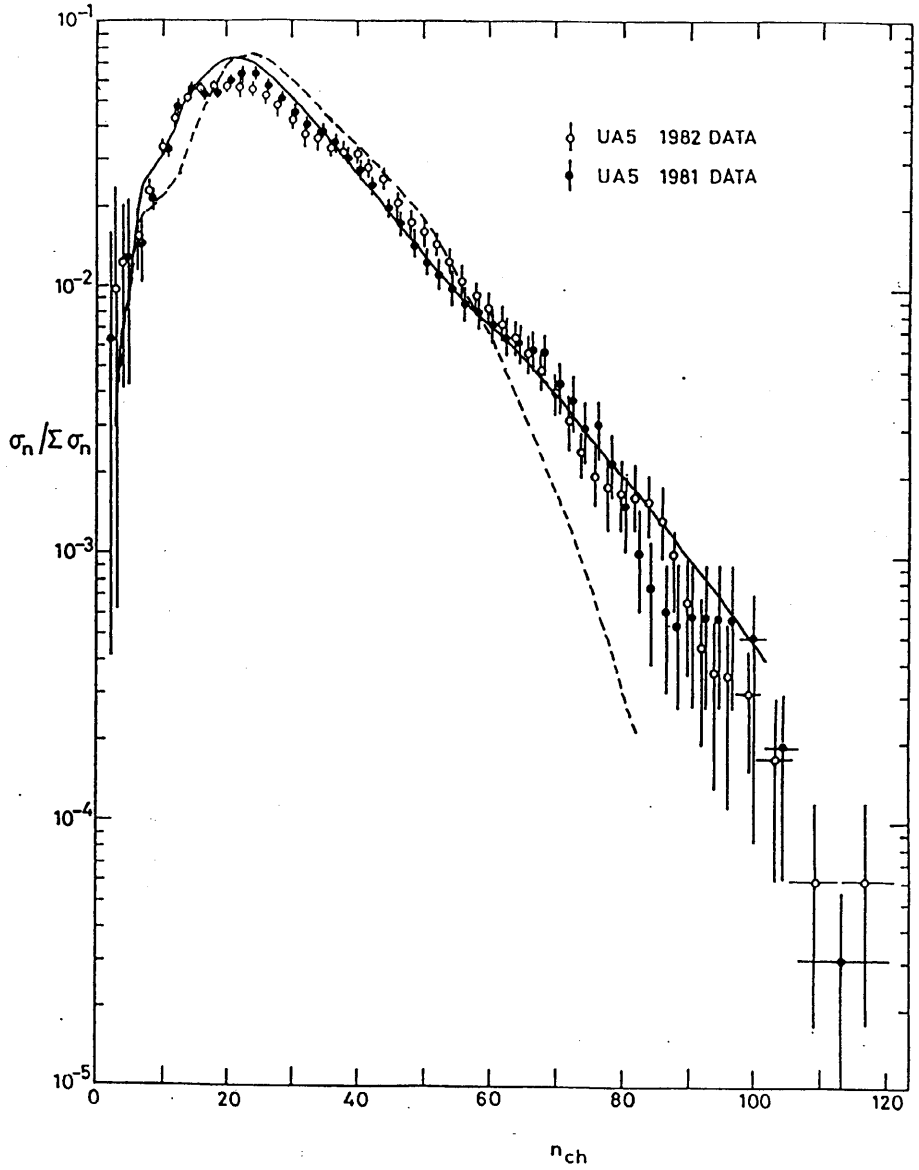
UA5 1982 DATA
UA5 1981 DATA
$\sigma_n / \Sigma \sigma_n$
n_{ch}
10^{-1}
10^{-2}
10^{-3}
10^{-4}
10^{-5}
0
20
40
60
80
100
120

FIG. 12

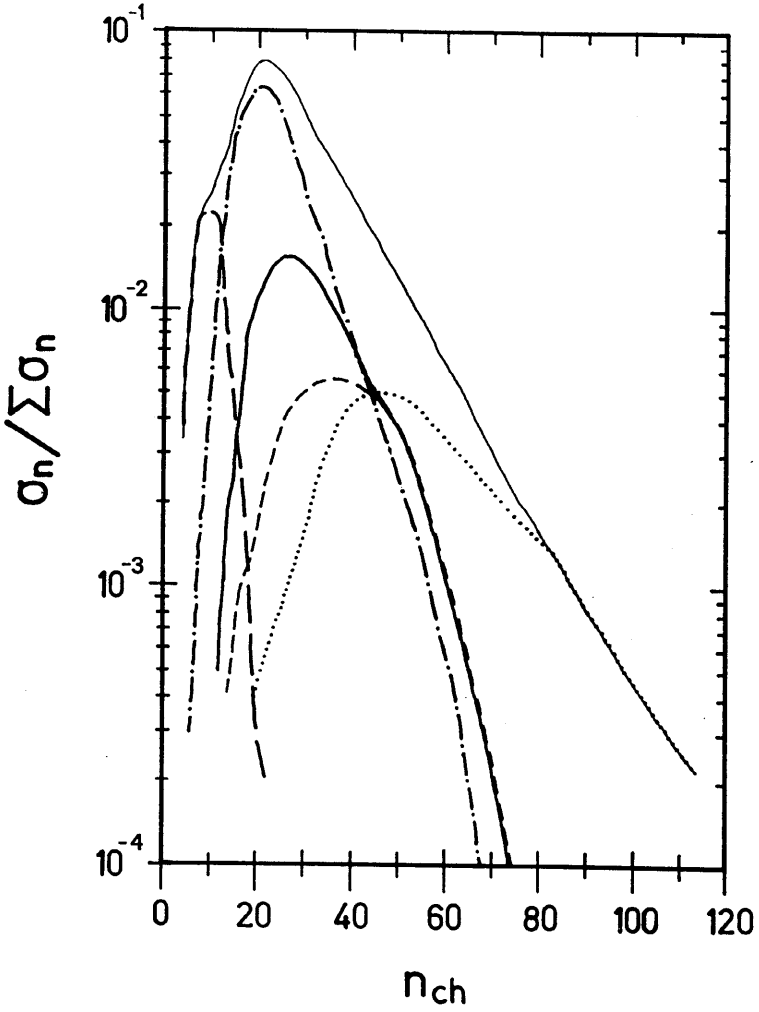
10^{-1}
10^{-2}
10^{-3}
10^{-4}
$\sigma_n/\sum\sigma_n$
0
20
40
60
80
100
120
n_{ch}

FIG. 13

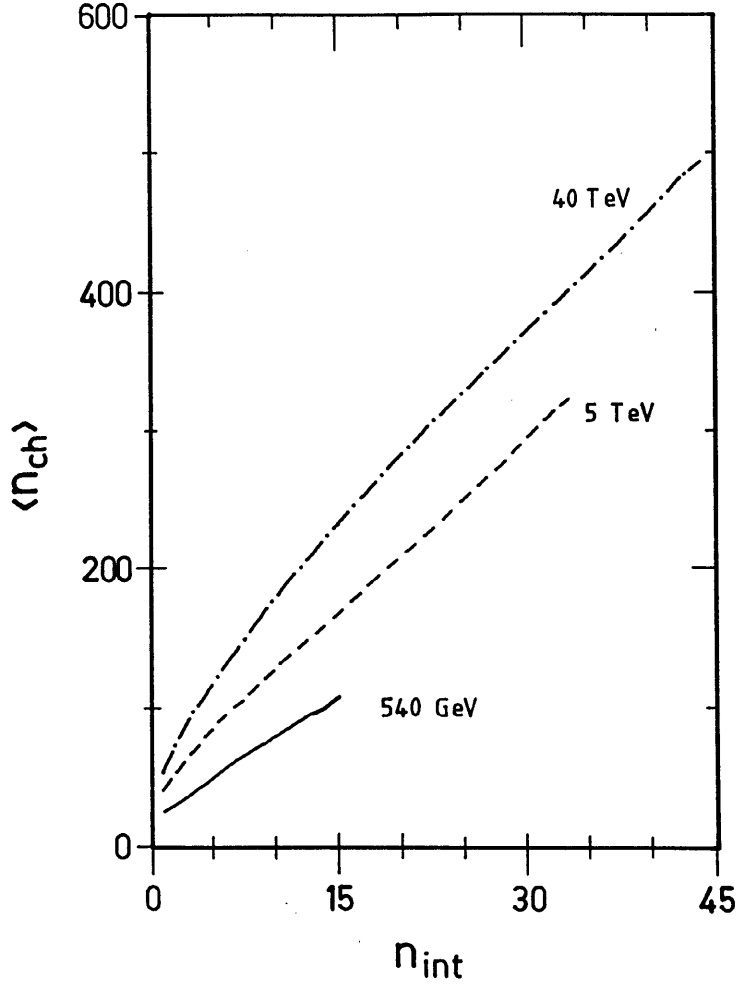
600
400
200
0
$\langle n_{ch} \rangle$
40 TeV
5 TeV
540 GeV
0
15
30
45
n_{int}

FIG. 14

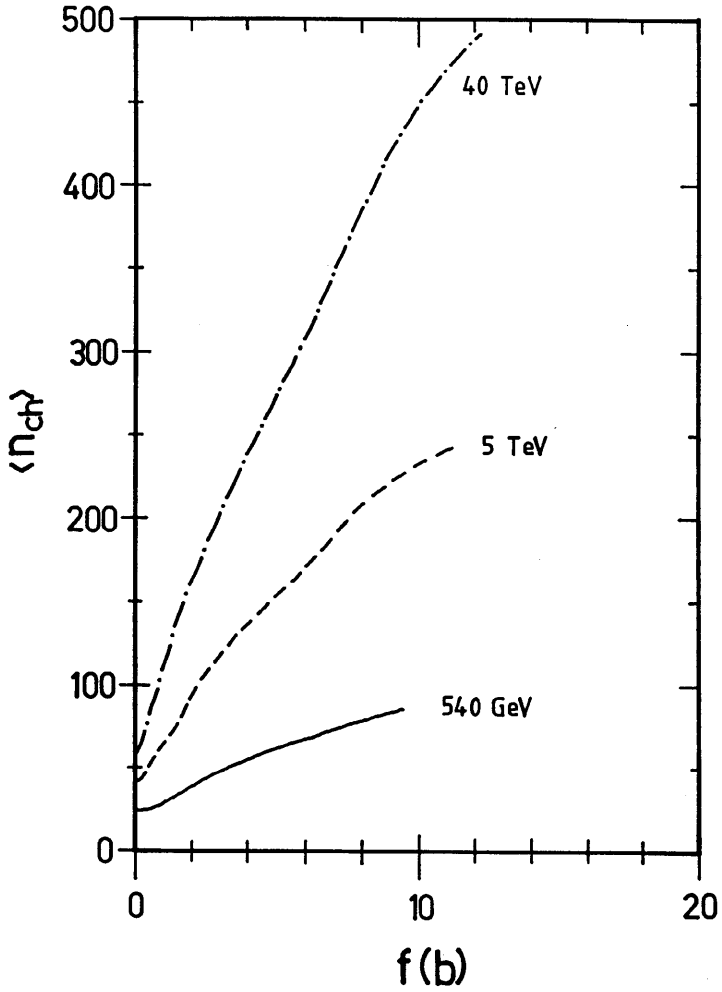
500
400
300
200
100
0
0
10
20
⟨n_ch⟩
f(b)
40 TeV
5 TeV
540 GeV

FIG. 15

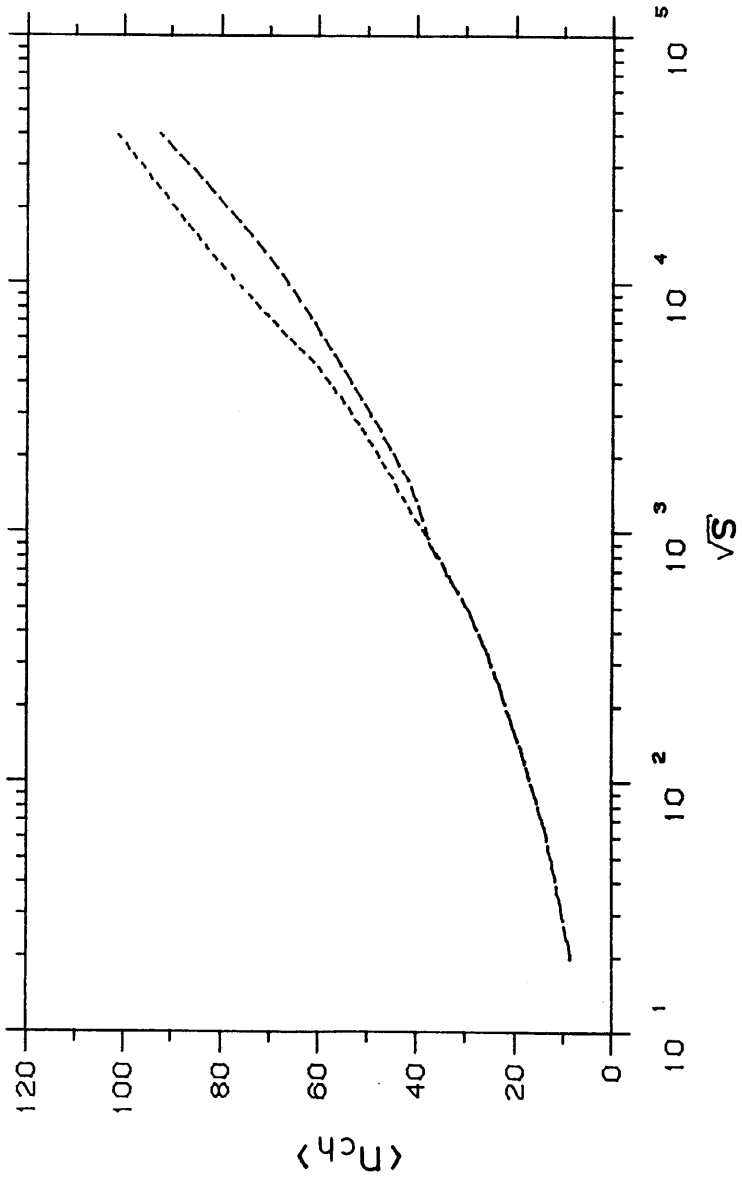
120
100
80
60
40
20
0
⟨n_ch⟩
10^1
10^2
10^3
10^4
10^5
√s

FIG. 16

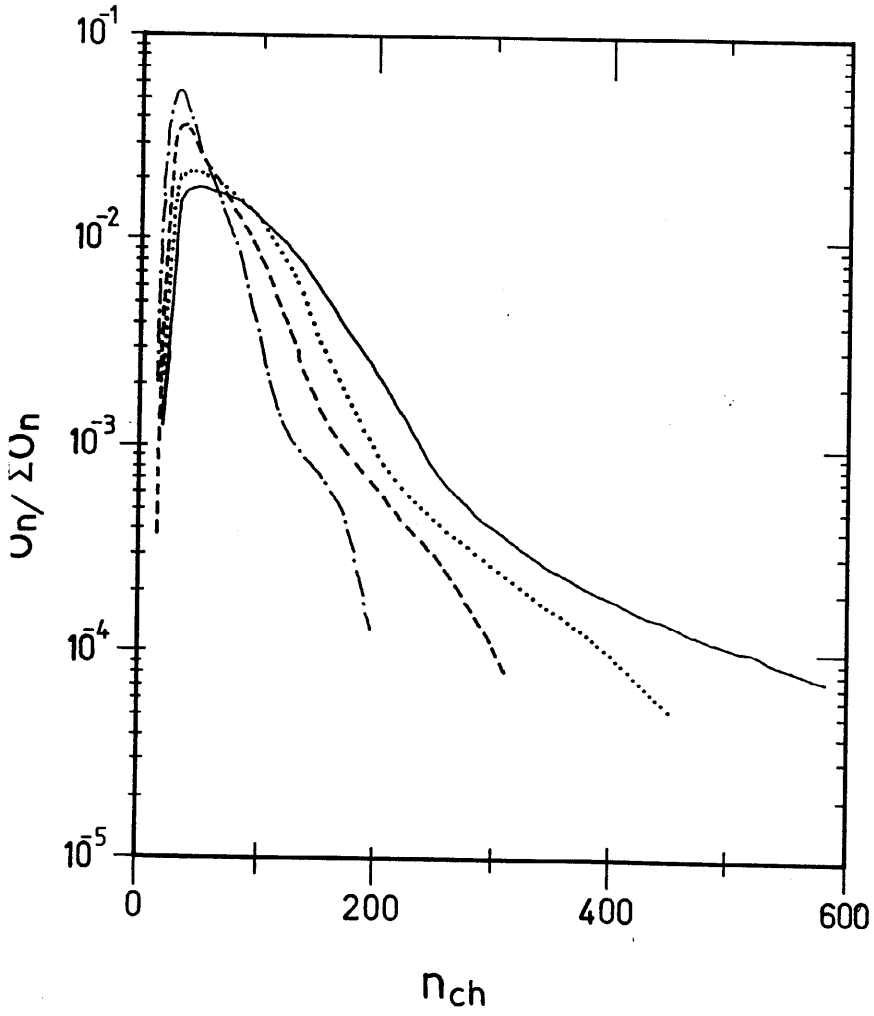
10^{-1}
10^{-2}
10^{-3}
10^{-4}
10^{-5}
$\sigma_n / \Sigma\sigma_n$
0
200
400
600
n_{ch}

FIG. 17

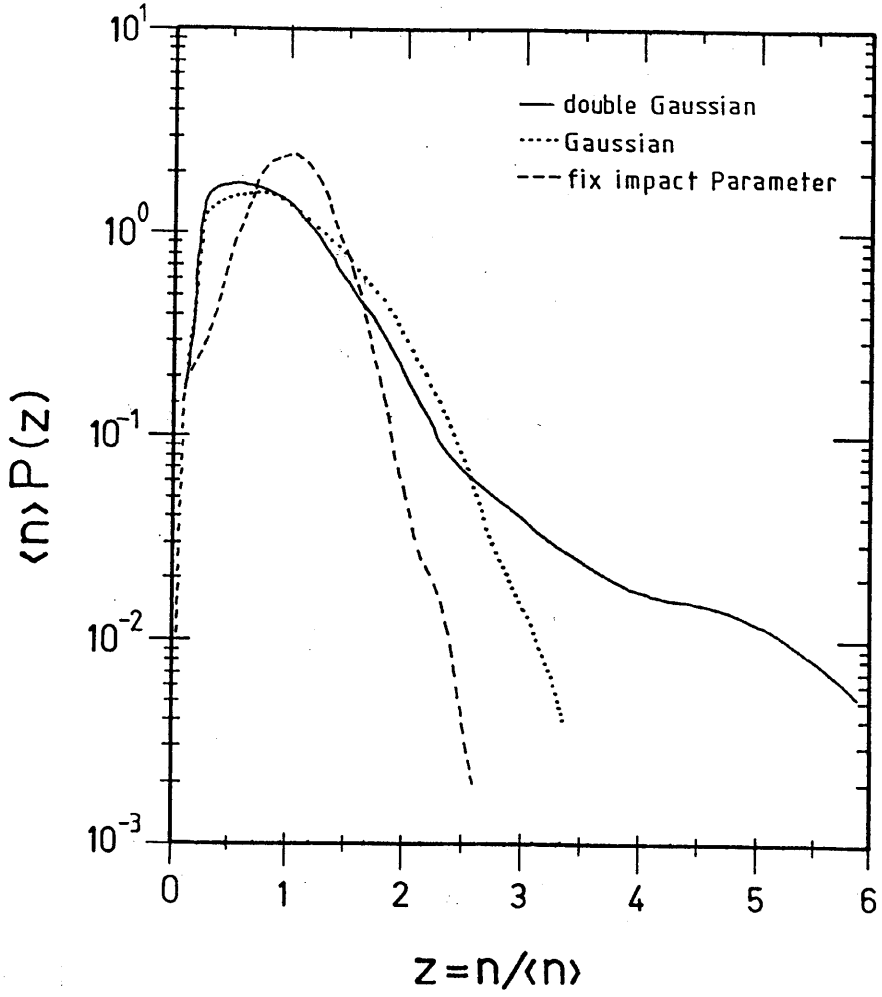
double Gaussian
Gaussian
fix impact Parameter
10^{1}
10^{0}
10^{-1}
10^{-2}
10^{-3}
$\langle n \rangle P(z)$
0
1
2
3
4
5
6
$z = n/\langle n \rangle$

FIG. 18

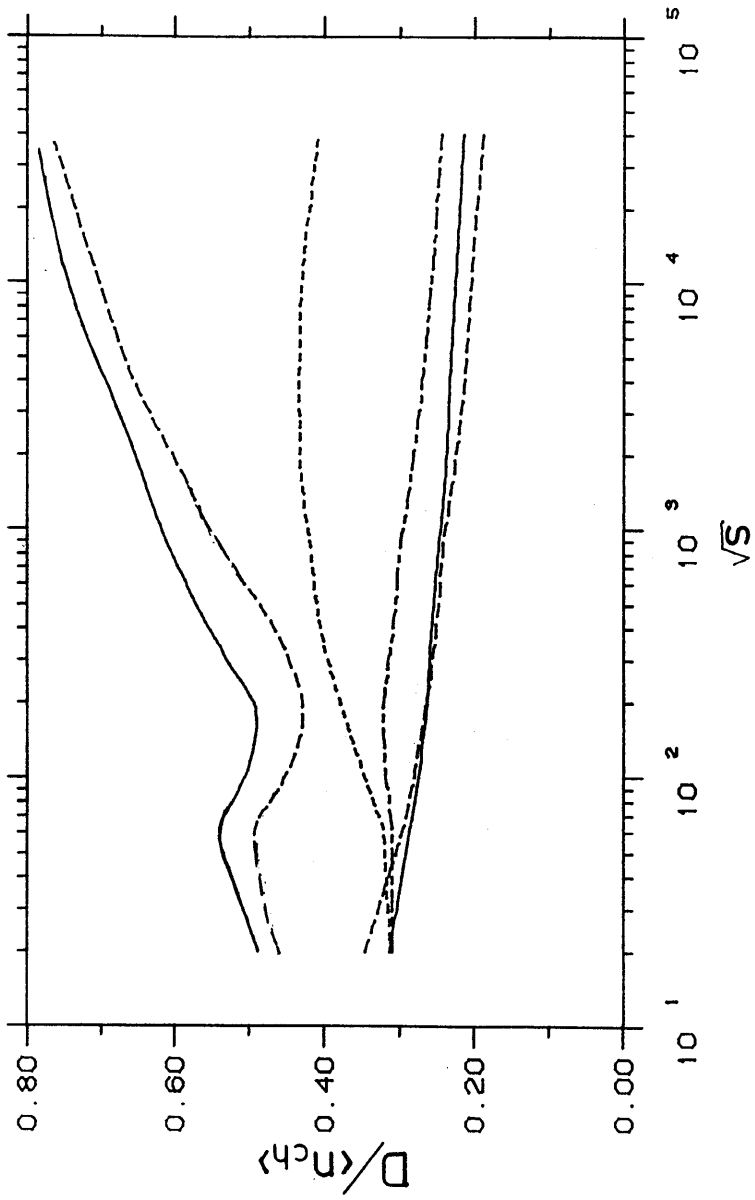
D/⟨n_ch⟩
0.00
0.20
0.40
0.60
0.80
10^1
10^2
10^3
10^4
10^5
√s

FIG. 19

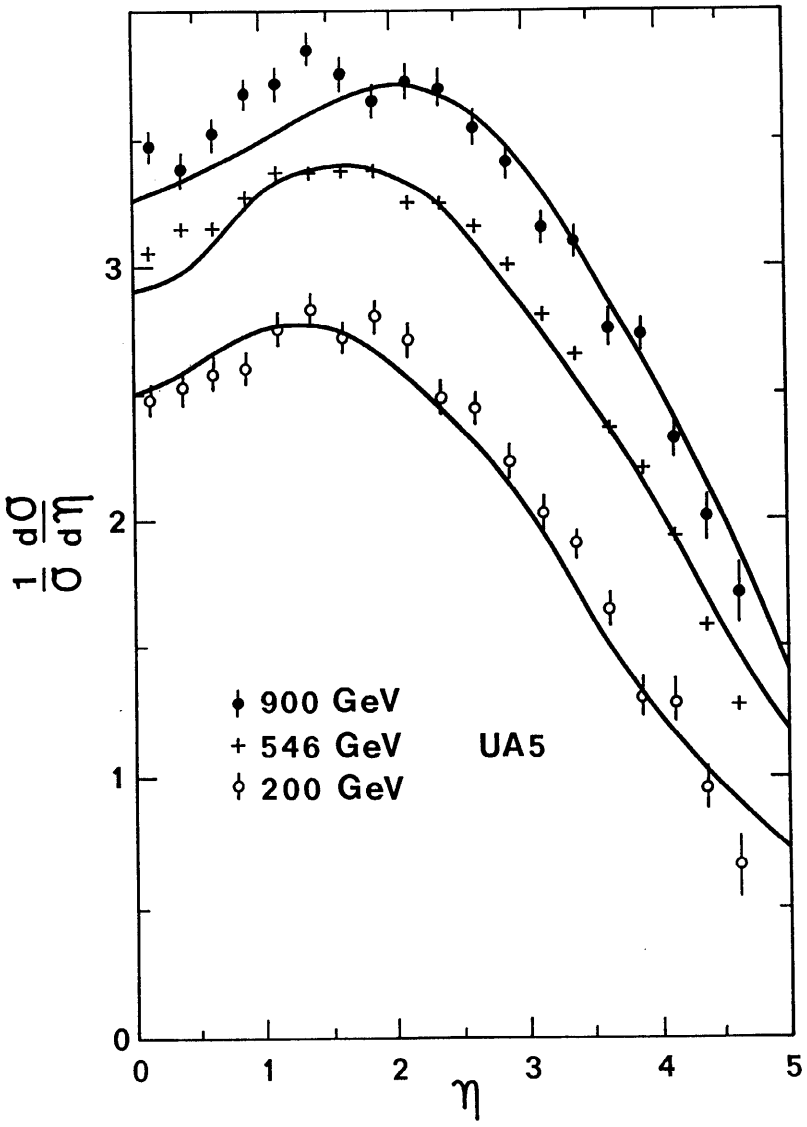
1/σ dσ/dη
0
1
2
3
0
1
2
3
4
5
η
900 GeV
546 GeV
200 GeV
UA5

FIG. 20

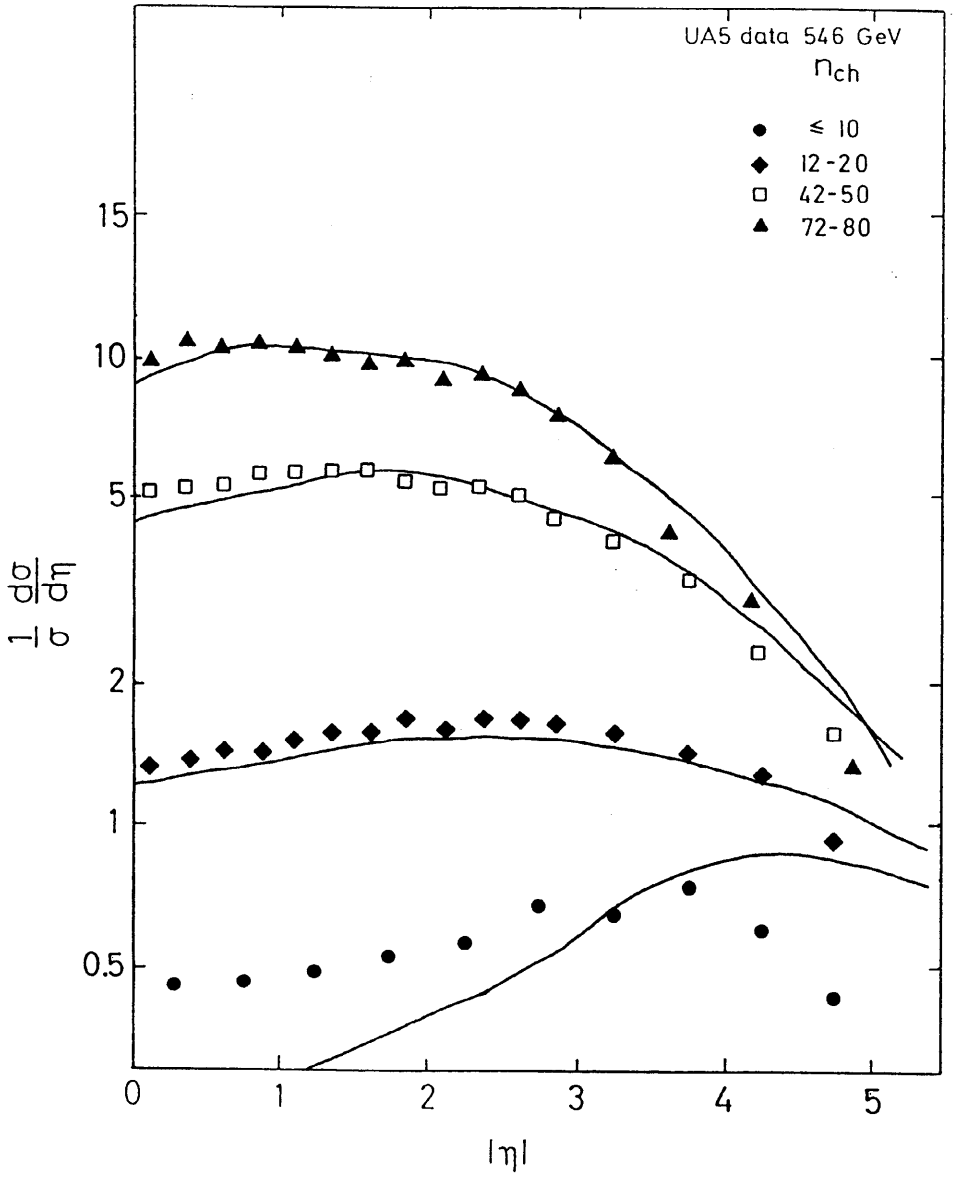
UA5 data 546 GeV
n_{ch}
≤ 10
12-20
42-50
72-80
$\frac{1}{\sigma}\frac{d\sigma}{d\eta}$
$|\eta|$

FIG. 21

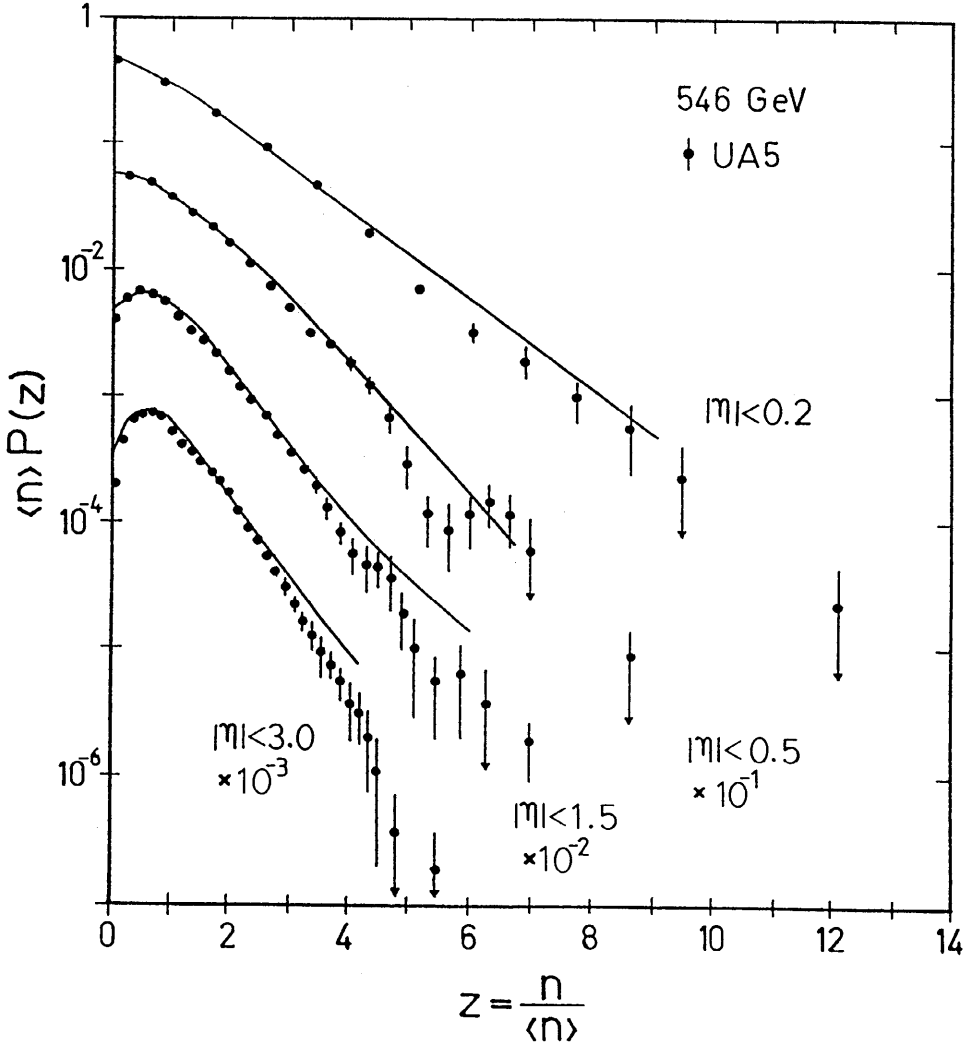
546 GeV
UA5
$|\eta|<0.2$
$|\eta|<3.0$
$\times 10^{-3}$
$|\eta|<1.5$
$\times 10^{-2}$
$|\eta|<0.5$
$\times 10^{-1}$
$\langle n\rangle P(z)$
$z=\frac{n}{\langle n\rangle}$

FIG. 22

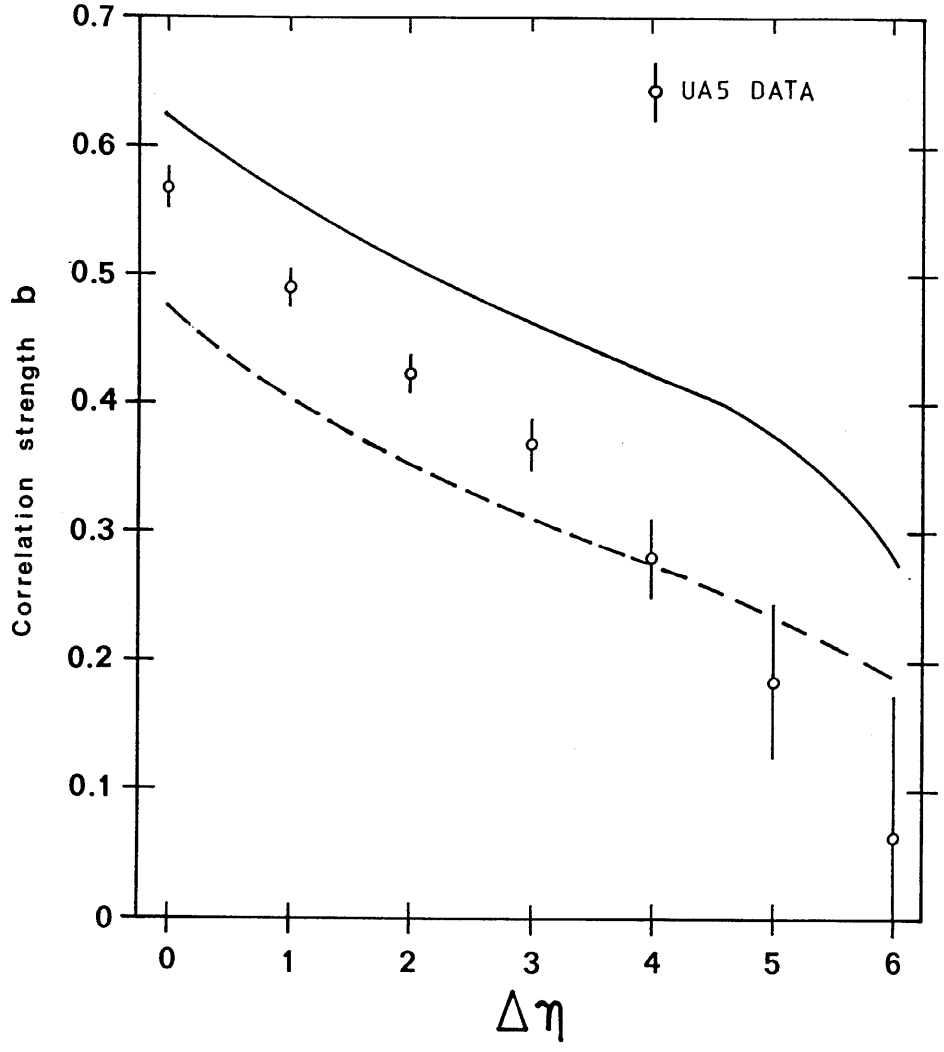
UA5 DATA
Correlation strength b
0.7
0.6
0.5
0.4
0.3
0.2
0.1
0
0
1
2
3
4
5
6
Δη

FIG. 23

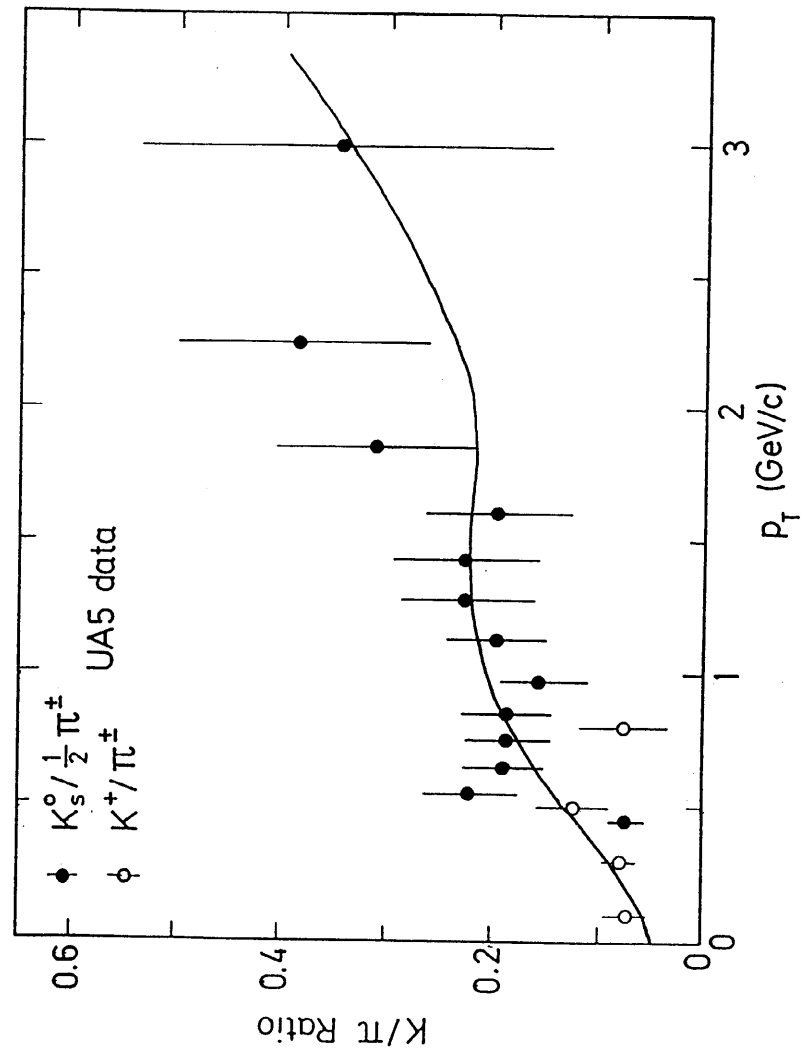
$K_s^o/\frac{1}{2}\pi^{\pm}$
$K^+/\pi^{\pm}$
UA5 data
K/π Ratio
0.6
0.4
0.2
0
0
1
2
3
P_T (GeV/c)

FIG. 24

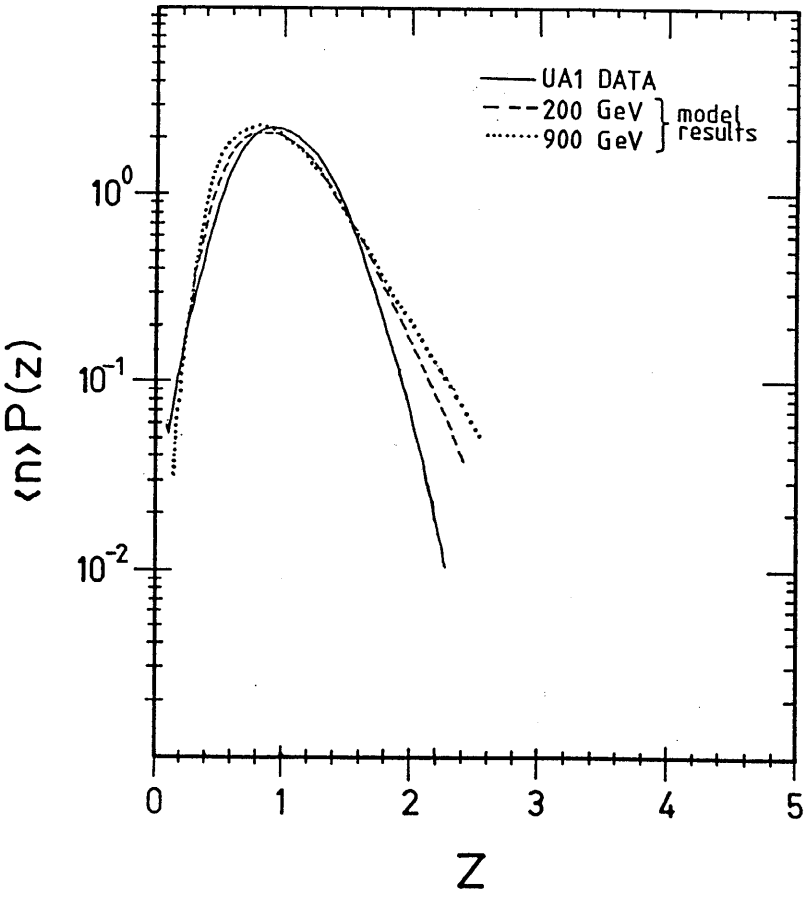

FIG. 25 A

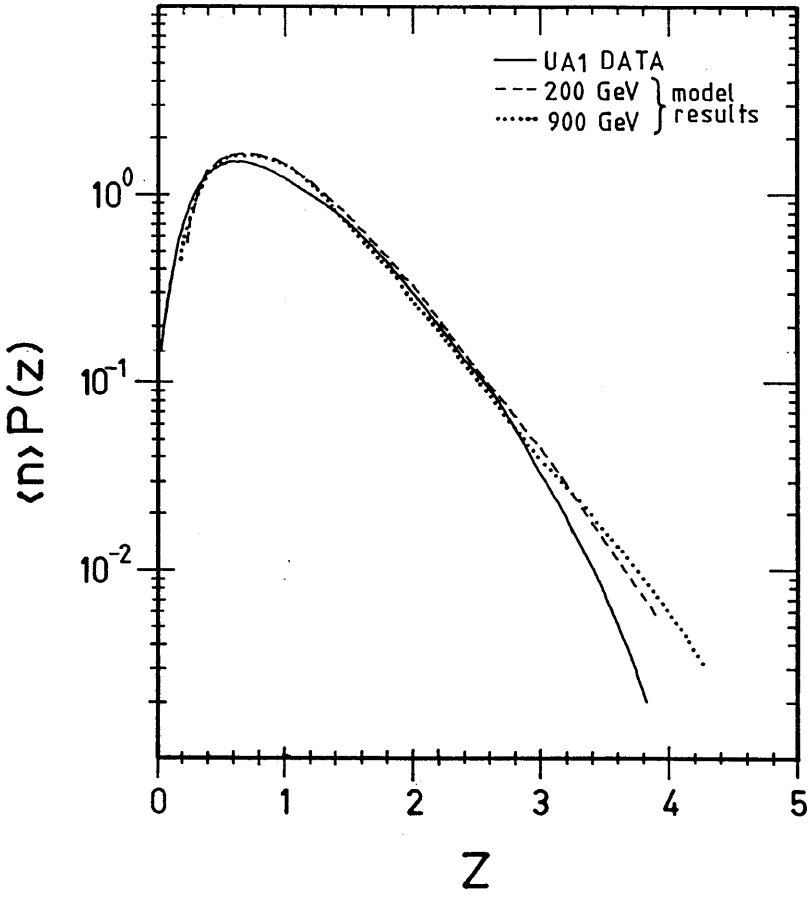

FIG. 25 B

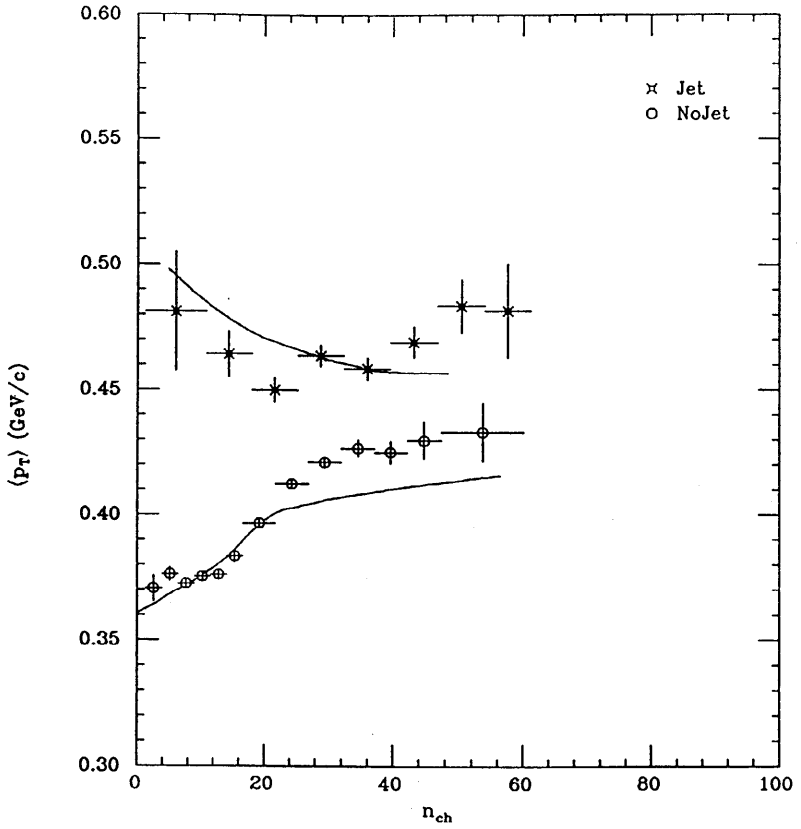
Jet
NoJet
0.60
0.55
0.50
0.45
0.40
0.35
0.30
0
20
40
60
80
100
$\langle p_T \rangle$ (GeV/c)
n_{ch}

FIG. 26

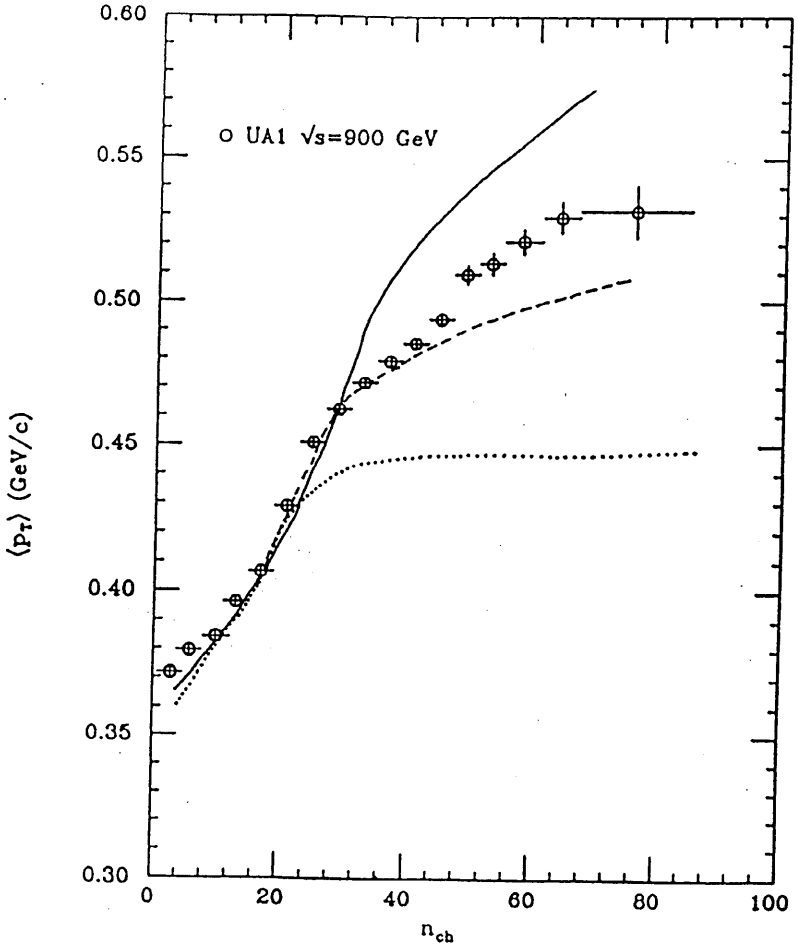
UA1 √s=900 GeV
0.60
0.55
0.50
0.45
0.40
0.35
0.30
0
20
40
60
80
100
$\langle p_T \rangle$ (GeV/c)
n_{ch}

FIG. 27

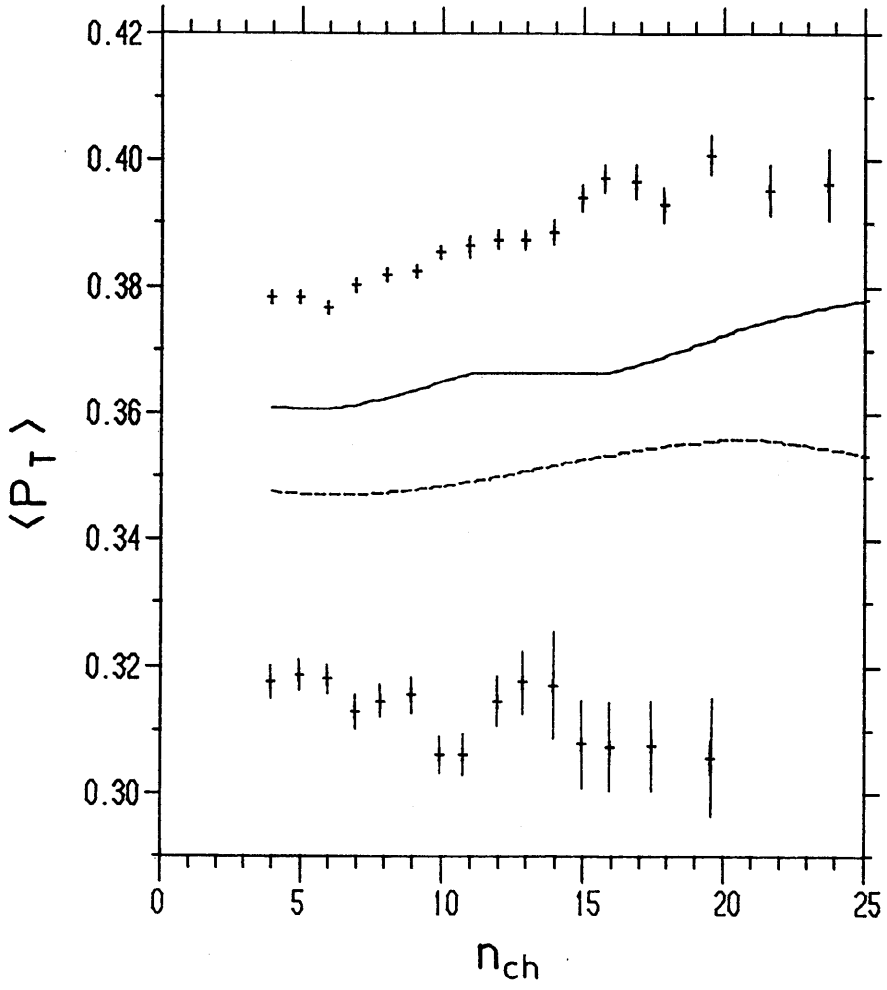
0.42
0.40
0.38
0.36
0.34
0.32
0.30
⟨P_T⟩
0
5
10
15
20
25
n_ch

FIG. 28

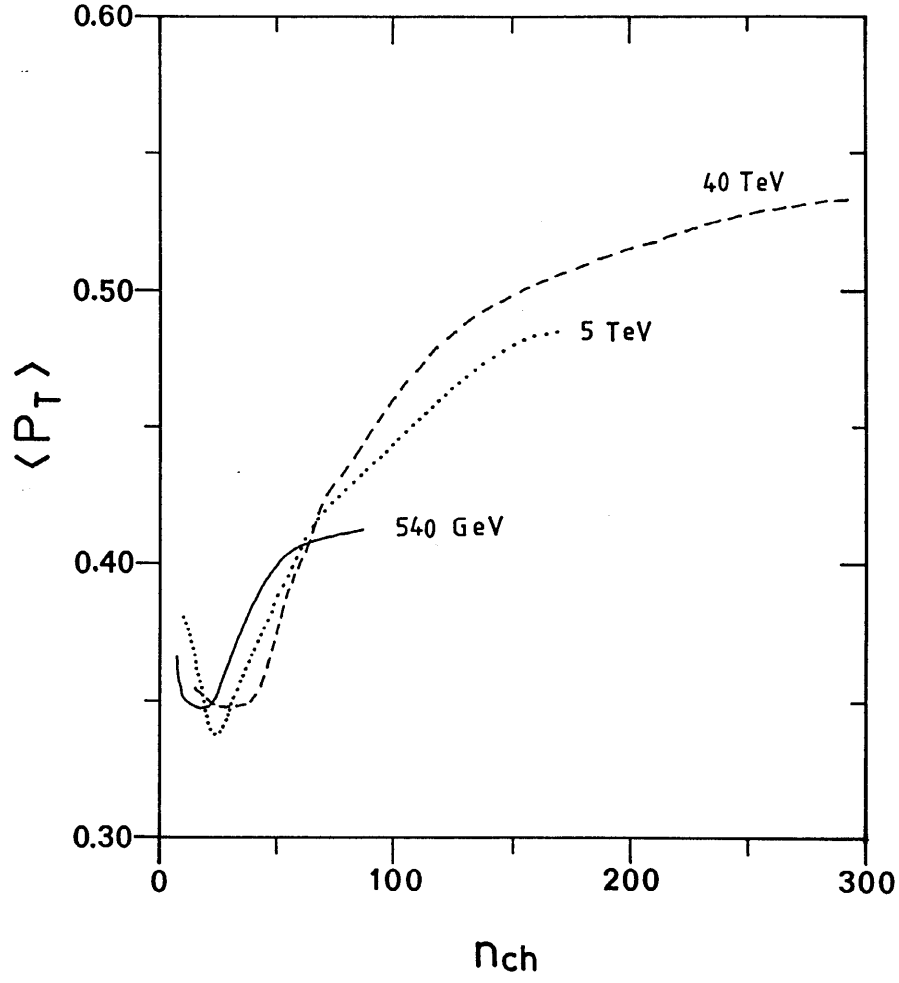
0.60
0.50
0.40
0.30
⟨P_T⟩
40 TeV
5 TeV
540 GeV
0
100
200
300
n_ch

FIG. 29

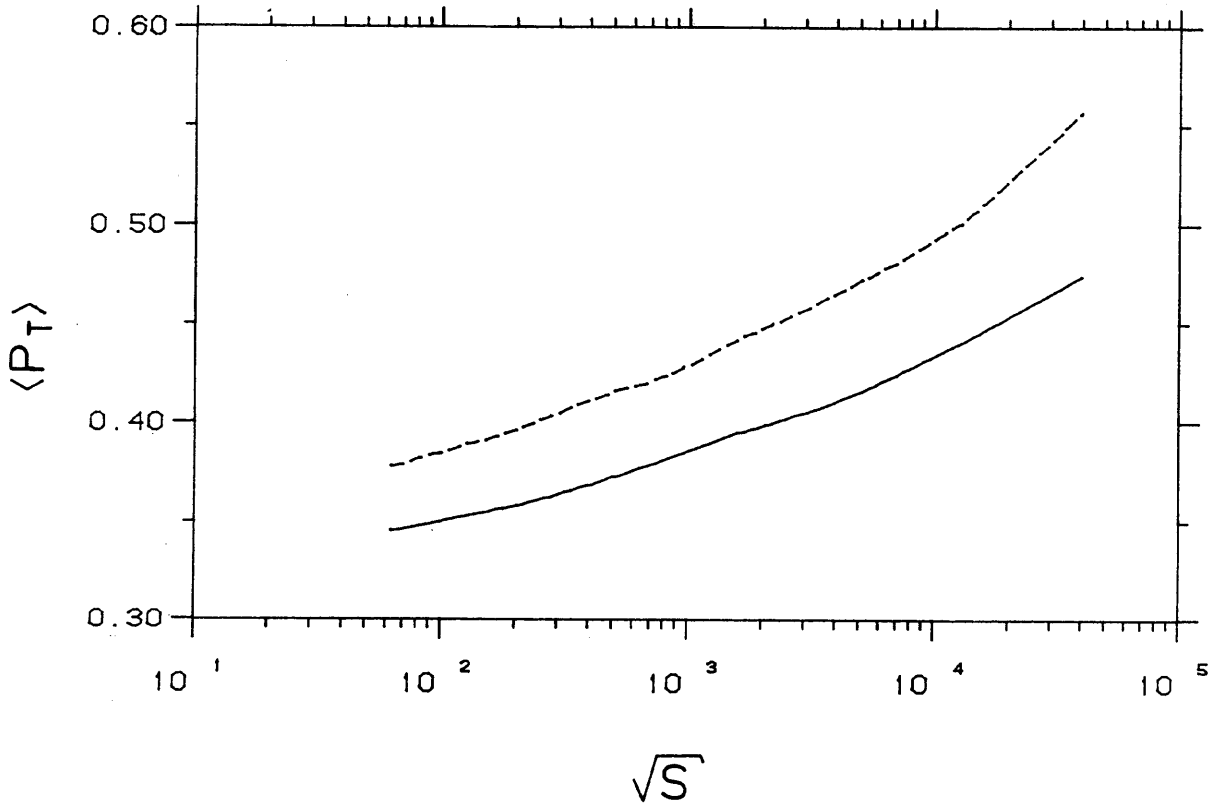
0.60
0.50
0.40
0.30
⟨P_T⟩
10^1
10^2
10^3
10^4
10^5
√S

FIG. 30

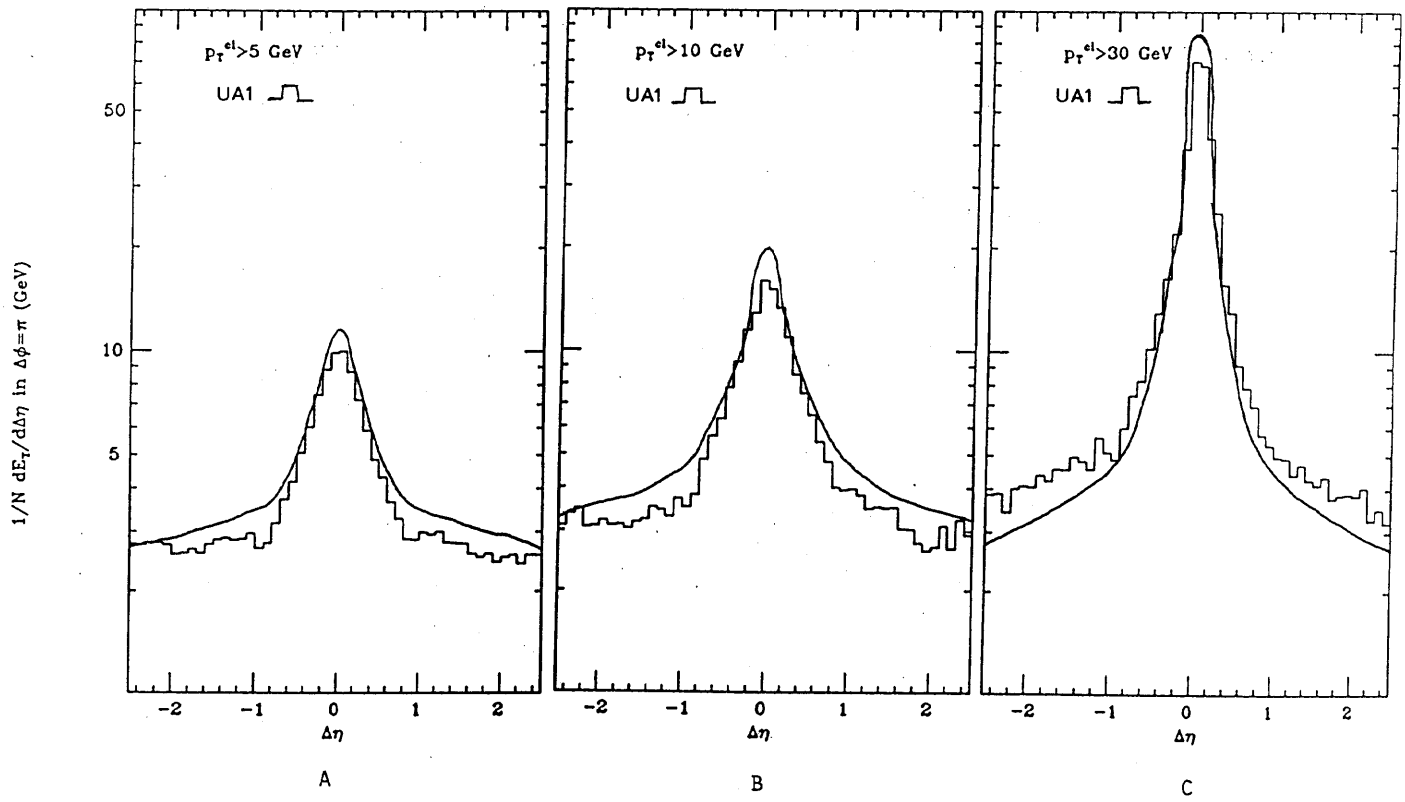
p_T^el>5 GeV
UA1
p_T^el>10 GeV
UA1
p_T^el>30 GeV
UA1
50
10
5
1/N dE_T/dΔη in Δφ=π (GeV)
-2
-1
0
1
2
Δη
A
B
C

FIG. 31

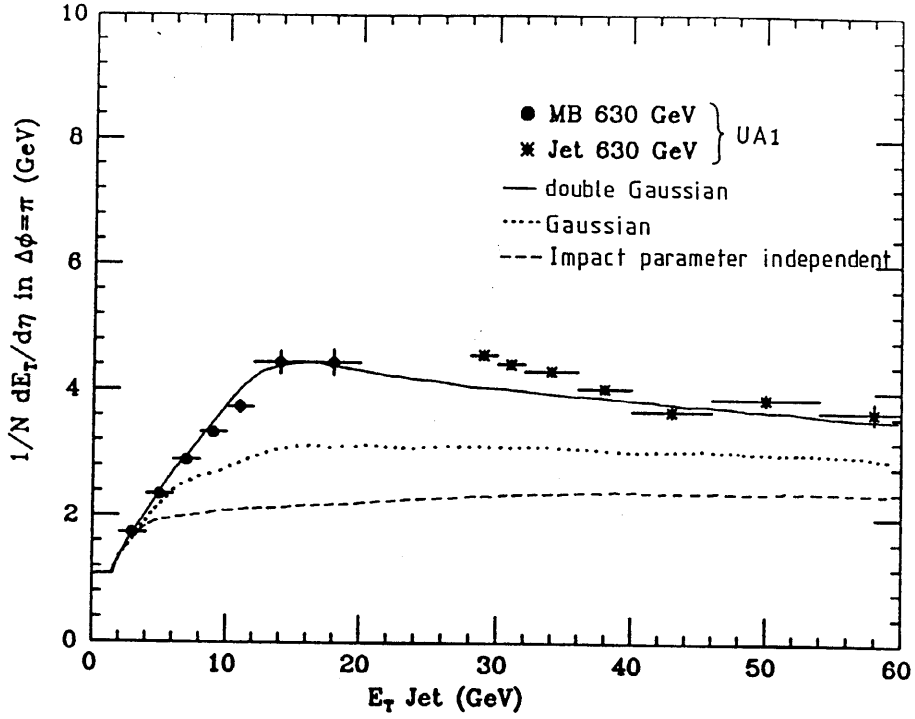
MB 630 GeV
Jet 630 GeV
UA1
double Gaussian
Gaussian
Impact parameter independent
1/N dE_T/dη in Δφ=π (GeV)
E_T Jet (GeV)
0
2
4
6
8
10
0
10
20
30
40
50
60

FIG. 32

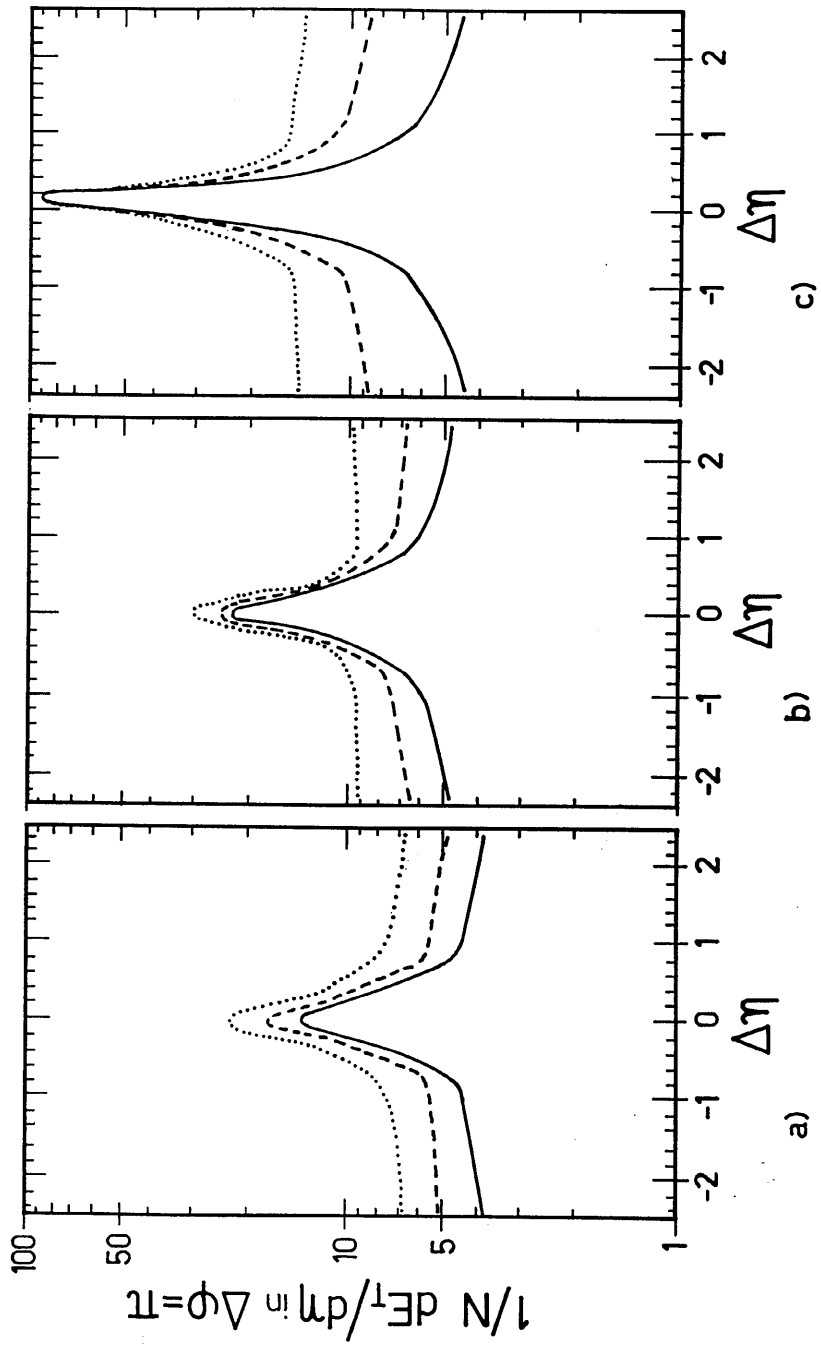
1/N dE_T/dη in Δφ=π
100
50
10
5
1
-2
-1
0
1
2
Δη
a)
b)
c)

FIG. 33

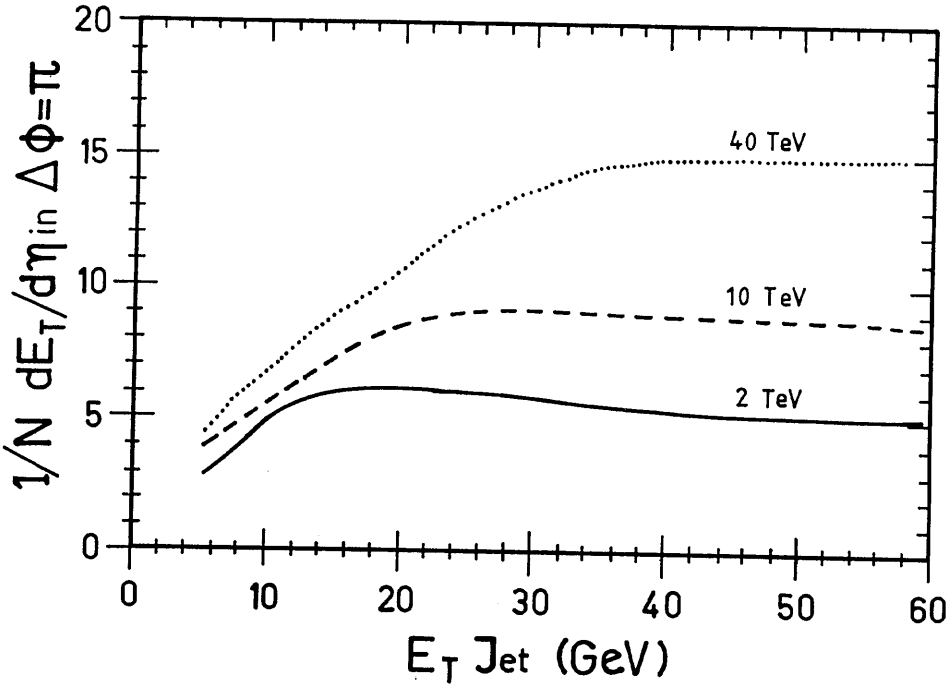
20
15
10
5
0
0
10
20
30
40
50
60
1/N dE_T/dη_in Δφ=π
E_T Jet (GeV)
40 TeV
10 TeV
2 TeV

FIG. 34